Quantum Molecular Dynamics of Ultrafast Processes in Large Polyatomic Systems

Pavel Jungwirth*,† and R. Benny Gerber‡,§

J. Heyrovský Institute of Physical Chemistry, Academy of Sciences of the Czech Republic, Dolejskova 3, 18223 Prague 8, Czech Republic, Department of Physical Chemistry and The Fritz Haber Center for Molecular Dynamics, The Hebrew University of Jerusalem, Jerusalem 91904, Israel, and Department of Chemistry, University of California, Irvine, California 92697-2025

Received November 25, 1998 (Revised Manuscript Received February 18, 1999)

Contents

I. Introduction

In the past few years, there has been a great surge of interest and activity in the quantum mechanical description of dynamical processes in large molecular systems. Until very recently, quantum treatment of chemical dynamics was confined to few-atom systems.[1−9] It is now state-of-the-art for triatomic and tetra-atomic systems and typically provides results far superior in precision and experimental relevance to those obtained using classical molecular dynamics. It is well-recognized that quantum effects such as tunneling and zero-point motions may also play an important role in dynamical processes in polyatomic systems; however, the usual theoretical treatment based on classical mechanics misses them completely. Efforts are currently being made by a wide variety of approaches to overcome the present computational limitations and to treat the quantum dynamics of processes in polyatomic molecules, large clusters, and condensed phases which carry enormous importance in chemistry. This research area is driven and motivated by the innovative experimental techniques that are being introduced and challenge, in particular, the understanding of ultrafast processes taking place at the femtosecond time scale.[10−12]

The present review aims at a two-fold purpose: To survey the methods and computational approaches currently available for the quantum treatment of chemical dynamics in many-atom systems and to illustrate how these theoretical tools are employed for the interpretation of experiments. In addition to drawing the landscape of different existing methods with their successes and limitations, we show their record of interactions with experiments, which are discussed in some detail. This review also focuses on the important open problems in this young area of research and on the possible directions of its future development.

The paper is organized as follows. In the following section, we the scene by formulating and outlining an answer to the basic question: Why and when is quantum treatment of the dynamics of polyatomic systems necessary? In section III, we briefly present current techniques for "numerically exact" quantum propagations in small systems. This topic has already been addressed by other reviewers;[8,13−16] therefore, we do not aim for a complete account but rather for showing concepts important for development of methods applicable to polyatomic systems. These methods, which due to the large number of degrees of freedom involved employ different kinds of approximations, are presented in detail in section IV. Section V

* To whom correspondence should be addressed. E-mail: jungwirt@jh-inst.cas.cz.
† Academy of Sciences of the Czech Republic.
‡ The Hebrew University of Jerusalem.
§ University of California—Irvine.

10.1021/cr9800210 CCC: $35.00
Published on Web 04/30/1999

Pavel Jungwirth (born 1966) graduated in physics at the Charles University of Prague in 1989. He finished his doctoral thesis in physical chemistry (particularly molecular simulations) at the Heyrovský Institute in Prague under the supervision of Professor Rudolf Zahradník in 1993. He was a visiting scientist at the University of Fribourg and University of Geneva performing quantum chemistry calculations in 1991–1992. In 1994–1995 he was a Golda Meir Fellow at the Hebrew University of Jerusalem and a Postdoctoral Fellow at the University of California at Irvine, working with Professor R. Benny Gerber in the field of quantum molecular dynamics. Since 1995 he has been a research group leader at the Heyrovský Institute and at the same time has been teaching an advanced course in computer simulations at the Charles University. His main scientific interests concern quantum simulations, spectroscopy and control of ultrafast processes in polyatomic systems, vibrational and rotational structure of cryogenic molecular clusters, and construction of potential energy surfaces and nonadiabatic couplings for large chemical systems.

R. Benny Gerber was born in 1944 and graduated in Chemistry from the Hebrew University of Jerusalem in 1965. He did his doctoral thesis in theoretical chemistry under C. A. Coulson at the University of Oxford, obtaining a D.Phil. in 1968. He was a Postdoctoral Research Associate with Martin Karplus at Harvard University in 1968–1969. He has been at the Hebrew University of Jerusalem since 1976 and holds the Saerree K. and Louis P. Fiedler Chair in Chemistry there. Since 1990, he has held this position jointly with an appointment as Professor of Chemistry at the University of California at Irvine. His current research interests are (1) vibrational spectroscopy and potential energy determination for large molecular systems (biomolecules, hydrogen-bonded clusters, etc.), (2) photochemical reactions and energy transfer in clusters and in solids, (3) quantum simulation methods for many-atom systems, and (4) processes at disordered solid and liquid surfaces.

provides a description of numerous applications of quantum dynamical computational techniques to interesting and experimentally relevant ultrafast processes in polyatomic systems. Finally, section VI provides a summary and conclusions and section VIII an extensive list of references.

II. Quantum Treatment of Chemical Dynamics—Why and When?

Due to its immense success in describing and predicting dynamical properties of atomic and molecular systems, quantum mechanics has proven to be the proper theoretical tool in this field. For diatomic to tetra-atomic systems this knowledge has already been projected to accurate computational techniques, the results of which correlate quantitatively with experimental predictions. On the other hand, it is a common practice today to describe processes in larger systems with up to several hundred thousands of atoms by classical molecular dynamics (MD) simulations.[17−20] Does that mean that it is no longer necessary to employ quantum mechanics when the size of the system reaches five atoms? There is no obvious reason the answer should be yes, and the arguments for retreating for large systems to classical mechanics are computational rather than physical. The key problem is the scaling of the computational effort with system size, which is mild (low-order polynomial) for classical MD but very unfavorable (exponential) for the exact numerical solution of the time-dependent Schrödinger equation.[21]

An obvious problem with classical simulations is that by definition they miss all quantum effects. A measure of the quantum character of a given particle is its de Broglie wavelength, which is inversely proportional to the particle momentum. Therefore, quantum treatment becomes inevitable whenever light atoms or low temperatures are involved, like, e.g., in matrix isolation or supersonic jet expansion experiments. Here, nonclassical effect such as zero-point motions, tunneling, or nonadiabatic transitions can play a dominant role in dynamical processes. Moreover, many observable properties, such as absorption or resonance Raman intensities in molecules, clusters, and condensed phases or state-to-state transitions in atom scattering from large molecules cannot be treated quantitatively on a classical footing and quantum description becomes necessary.[22] Quite generally, for molecular probes that look primarily at a local response (e.g., excitation of a single bond), quantum effects are roughly of the same importance for large and small systems in comparable conditions. Other methods probe properties proportional to the system size (such as the total kinetic energy) where the quantum effects tend to be less important in large systems.

Processes in small and large molecules often differ from each other significantly due to the more statistical behavior of the latter systems. Namely, due to effects such as intermolecular vibrational redistribution, measurables such as differential cross-sections are hard to extract experimentally for processes in polyatomic systems. Rather, "averaged" characteristics such as absorption profiles or energy distributions are typically provided by the experiment. In other words, different questions are asked by the experimentalists for small and large systems, those for the latter being of a more averaged and statistical character. This is certainly good news for theory which for large systems has to introduce, on the

quantum mechanical level, approximations. As shown in the following sections, simple methods based on the separable mean-field approximation are by construction quite reliable for extracting the overall properties of large systems. Provided that detailed state-to-state observables are to be reproduced, computationally more involved methods which go beyond separability of individual dynamical degrees of freedom usually have to be employed.

III. Quantum Dynamical Simulations of Small Systems

Time-dependent quantum simulation methods have been extremely successful in interpreting dynamical phenomena in small, diatomic to tetra-atomic systems, providing results in quantitative accord with experiment in cases where the underlying interaction potentials are known to sufficient accuracy.[1,9] The power of these methods, as compared to time-independent approaches, is due to their numerical efficiency, especially for the description of very fast processes, as well as due to their simple physical interpretation. By following events through time, these methods naturally correspond to experiment and to our intuitive understanding of the chemical dynamics. Thus, by simple visualization of the time-dependent wave functions, physical insight is directly provided which is an advantage in comparison to time-independent calculations.

The goal is to solve numerically the time-dependent Schrödinger equation

$$i\hbar\frac{\partial\Psi(\vec{x},t)}{\partial t} = (\hat{T} + \hat{V}(\vec{x}))\Psi(\vec{x},t) \qquad (1)$$

for the system under study. Here, $\Psi(\vec{x},t)$ is the wave function depending on the spatial degrees of freedom of atomic nuclei $\vec{x}$ and on time t and the Hamiltonian $\hat{H}$ consists of a kinetic part $\hat{T}$ and a potential part $\hat{V}$. The computational task has three parts—to spatially discretize the wave function, to perform the Hamiltonian operation, and to propagate the initial wave function in time. Since this problem has already been addressed in previous reviews,[8,13−16] we do not aim here for an exhaustive account of existing methods. The purpose of this section is rather to provide the reader the necessary background to be able to follow the description of approximate quantum simulation techniques presented in the next section.

The simplest and most robust spatial discretization technique is the grid representation where the wave function is discretized on an equidistant spatial grid.[16] Clearly, the grid should be large enough to encompass the whole wave function during the time period under study, and the number of grid points should be sufficient for the discretized wave function being a faithful representation of the continuous function. In one dimension, this discretization means evaluating the wave function $\Psi(x,t)$ on a set of points $\{x_1,...,x_K\}$. In more dimensions, the number of grid points equals K^N, where N is the dimensionality of the problem and K is the number of grid points per degree of freedom. We immediately see here the unfavorable scaling of the numerically exact methods with system size, the so-called exponential catastrophe, which effectively prevents such calculations for larger systems.

Although the equidistant grid representation is the most general and widely applicable, it is often computationally more efficient to work with more specialized discretizations of the wave function. This typically means expanding the wave function in a series of suitable orthogonal basis functions.[15] For bound-state problems where the system moves close to the bottom of the potential well, vibrational degrees of freedom are often efficiently described by basis set expansions using, e.g., harmonic or Morse oscillator eigenfunctions. For the description of rotational and hindered rotational motions, it is usually advantageous to use expansions into the series of the free rotor eigenfunctions. Although in practice it is always necessary to truncate the basis set expansion, the above methods, in principle, introduce an infinite complete set of functions. New approaches based on the discrete variable representation (DVR), which have proven to be computationally very efficient, work on the other hand from the very beginning with a finite basis set, and the evaluation of the corresponding matrix elements is based on collocation schemes.[23−25]

The next tasks are to perform the Hamiltonian operation on the wave function and to propagate the wave function, i.e., discretize it in time. We present here the basic ideas for the equidistant spatial grid representation where things are most transparent, but the same derivations can be done also for the basis set and DVR representations. The potential part $\hat{V}\Psi$ of the Hamiltonian operation is straightforwardly performed via point-by-point multiplication over the spatial grid since the potential energy operator is local in the coordinate space. On the other hand, the action of the kinetic energy operator $\hat{T} = -\hbar^2\Delta/(2m)$ on the wave function is more difficult to calculate. The most consistent and accurate approach for evaluation of $\hat{T}\Psi$ is the Fourier method,[26,27] which dwells on the fact that the kinetic energy operator is local in the reciprocal momentum space. Therefore, the wave function is first transformed using a fast Fourier transform algorithm[28] into the momentum space. There, local multiplication by $p^2/(2m)$, where p is the momentum and m is the corresponding mass, is performed, followed by an inverse Fourier transform back to the coordinate space.

Formally, the solution of the time-dependent Schrödinger equation can be written as[14]

$$\Psi(t) = \hat{U}(t)\Psi(0) \qquad (2)$$

where the evolution operator $\hat{U}$ is defined as[14]

$$\hat{U}(t) = e^{-(i/\hbar)\int_0^t \hat{H}(t')\mathrm{d}t'} \qquad (3)$$

For time-independent Hamiltonians, this expression simplifies to

$$\hat{U}(t) = e^{-(i/\hbar)\hat{H}t} \qquad (4)$$

Since the action of the evolution operator on the initial wave function cannot be directly performed

(we do not know how to apply the exponential of the Hamiltonian on the wave function), for practical applications different types of expansions have to be employed.

Depending on how the discretization of the evolution operator is made, wave function propagators basically fall into two categories. Local methods break up the evolution operator $\hat{U}$ into small time increments $\delta\hat{U}$ which move the wave function from time t to $t + \delta t$. If the time step δt is small enough, the time dependence of the Hamiltonian (if any) can be neglected and a simple expansion of the short time evolution operator $\delta\hat{U}$ can be done. Global methods, on the other hand, use more sophisticated expansions of the evolution operator in terms of sets of orthogonal polynomials. The most widely used approach uses an expansion into a series of Chebyshev polynomials.[29] Provided a sufficient amount of terms is included, it can be shown that the Chebyshev method has a minimal residual error compared to almost all polynomial expansions.[14]

In general, the Chebyshev method, which converges exponentially with the number of expansion terms, is more reliable and accurate than the local approaches. Unfortunately, its principal advantage—the possibility of using very long time steps, is lost if the Hamiltonian is time-dependent. As shown in the next section, effective Hamiltonians used for approximate propagations of wave functions of large systems are always time-dependent. Global approaches tailored to time-dependent Hamiltonians exists, such as the (t,t') scheme,[4,30−32] which is related to the stationary formulation of the time-dependent Schrödinger equation,[33,34] or the Krylov−Lanczos subspace Chebyshev methods.[35,36] These methods are very efficient, however, only when the time dependence of the Hamiltonian is periodic, like in the cases of interactions between matter and light. In the following paragraphs, we review in more detail the two most commonly used local propagators—the second order differences (SOD)[13−14,26−27,37−38] and the split-operator (S−O)[13−14,39−40] methods.

The simplest quantum propagator follows from a symmetrized Taylor expansion of the short time evolution operator $\delta\hat{U}$, truncated at the first nontrivial term, leading to the following prescription for the SOD scheme[13−14,26−27,37−38]

$$\Psi(t + \delta t) \approx \Psi(t - \delta t) - 2\frac{i}{\hbar}\hat{H}\Psi(t)\delta t \qquad (5)$$

To initialize the SOD propagation, wave function at $t = 0$ and $t = -\delta t$ is required (see eq 5). The latter is usually constructed by propagating at $t = 0$ one-half-step backward using an unsymmetrized propagator, followed by a regular SOD half-step backward yielding $\Psi(-\delta t)$. Once initialized, the propagation continues as indicated by eq 5. It can be easily seen that the error of the SOD propagator scales as $(\delta t)^3$. Generally, very short time steps should be used, and due to accumulation of numerical errors, accurate long time SOD propagations are hardly possible.

The S−O method splits the short time evolution operator into its kinetic and potential part in a way that accounts for the leading term in the commutator between the kinetic and potential energy operators, neglecting all higher terms. This is achieved by dividing the time interval between t and $t + \delta t$ into two equal parts. For the first half-interval, the kinetic part is applied first followed by the potential part, while for the second half-interval, the order is reversed. This reads the following expression for the S−O approximation to the short time evolution operator[13−14,39−40]

$$\delta\hat{U}(t) = e^{-(i/\hbar)\hat{H}\delta t} \approx e^{-(i/2\hbar)\hat{T}\delta t}e^{-(i/\hbar)\hat{V}\delta t}e^{-(i/2\hbar)\hat{T}\delta t} \qquad (6)$$

Let us note at this point that the order of the kinetic and potential operators in the above formula can also be reversed yielding an equivalent S−O algorithm:

$$\delta\hat{U}(t) = e^{-(i/\hbar)\hat{H}\delta t} \approx e^{-(i/2\hbar)\hat{V}\delta t}e^{-(i/\hbar)\hat{T}\delta t}e^{-(i/2\hbar)\hat{V}\delta t} \qquad (7)$$

As in the case of the SOD propagator, the potential part of the action of the evolution operator on the wave function is carried out directly in the coordinate space while the kinetic energy part is performed in the momentum space using the fast Fourier transform. Compared to the SOD propagator, the S−O approach has the advantage of generally being more accurate, which allows for the use of a relatively longer time step. The S−O method is also quite robust and stable and is, therefore, the method of choice for many applications involving time-dependent Hamiltonians.

Let us stress at the end of this section that the quantum dynamical algorithms, the very basics of which have been outlined here, cannot be directly applied to dynamical processes in large polyatomic systems. Each additional degree of freedom multiplies the number of numerical operations in the propagation by a factor of K, where K is the number of grid points or basis functions necessary for the description of the given mode. On the basis of limitations of computer speed and memory, the largest systems that can be currently handled have at most four atoms or six coupled modes. As a result of the exponential scaling of numerical effort for the exact solution of the Schrödinger equation with system size, approximations have to be employed for large systems. Many of these approximate methods lead to effective low-dimensional propagations where the algorithms outlined above can be directly applied.

IV. Methods for Quantum Dynamical Simulations of Large Systems

Numerically exact quantum dynamical methods scale exponentially with the system size and are, therefore, applicable only to small, at present no larger than tetra-atomic, systems. The approximations which have to be adopted for any practical calculation for larger systems go along two general lines which are not completely independent. The first class of approximations leads to methods based on separability of the wave function into contributions of individual modes (Hartree approximation), while the second class invokes to a certain extent concepts from classical mechanics. The most straightforward mixed quantum-classical approach which can be

viewed as a bridge between methods for small and large systems simply treats a few crucial degrees of freedom quantum mechanically while the rest of the system is described within classical mechanics. To divide the system into quantum and classical parts, a certain degree of separability has to be assumed which shows the connection between the two lines of approximations. There are, however, many other methods where classical mechanics are employed in a subtler way and the whole system dynamics are treated approximately but essentially quantum mechanically. In this section we review the currently used approximate quantum dynamical methods.

A. Time-Dependent Self-Consistent Field (TDSCF) Method

The basic idea behind the TDSCF approach (also called the time-dependent Hartree method) is to find, using the time-dependent variational principle, the best single particle separable representation of the multidimensional time-dependent wave function. As a result, the exact interactions between individual degrees of freedom are approximated by their mean-field values. The TDSCF method was introduced by Dirac in the early quantum days;[41] however, first applications to atomic and molecular systems began only in the 1970−80s.[42−49]

Before going into more detail, we can immediately estimate the range of validity of the TDSCF method. Trivially, the method becomes exact for noninteracting degrees of freedom. If the couplings are weak, like in cases with significant separation in effective masses and frequencies of individual modes, the method is supposed to work very well. For stronger couplings, the TDSCF approach can still be a good short time approximation but it will tend to deteriorate in time. This deterioration can also be related to a general effect of the dynamical spreading of the wave function of large systems in time. The more delocalized the wave function is, the less faithful the mean-field approximation to the exact interaction potential tends to be. A very nice feature of the TDSCF method is that it works, as all mean-field approaches, better for larger systems where the averaging of the intermode interactions becomes more justified. There is, therefore, a large degree of consistency since the TDSCF method is exactly aimed at large systems where numerically exact calculations are not possible. Finally, it has recently been shown that for system−bath processes, TDSCF works very well for finite bath temperatures since the bath-induced noise tends to diminish the effect of system−bath correlations.[50]

The issue of couplings between individual degrees of freedom brings up the question of the optimal choice of coordinates. Unlike the numerically exact propagation, which is independent of the coordinate system, the TDSCF results may strongly depend on the particular coordinate choice. Clearly, the optimal choice should minimize the couplings between the modes.[51−55] Unfortunately, for large systems there is no variational optimization prescription available and the selection of good coordinates is a difficult task. Most recently, we suggested a simple method which allows one to choose the best coordinates from a given set.[56] Within this scheme the difference between the exact and mean-field potentials is monitored along a swarm of classical Wigner trajectories and the coordinate set of choice should then minimize this error measure. Involving only classical propagation, this coordinate optimization procedure, which works well for mildly quantal systems, is computationally extremely cheap and can easily be applied to very large systems.

Among coordinate sets which are practical (i.e., computationally simple especially for the kinetic energy evaluation), normal modes are usually a good choice for low-energy excitations. Within this approach the effect of overall rotations is neglected, which is often well justified for low-lying rotational states. On the other hand, highly energetic dissociative systems will be better described within the Cartesian coordinate framework, especially when the separations between the dissociating particles become large, approaching the free-particle limit.

The derivation of the TDSCF equations[46,49] starts with the factorization of the total wave function Ψ into a product of single-mode functions

$$\Psi(q_1,...,q_N,t) = \prod_{j=1}^{N} \phi_j(q_j,t) \tag{8}$$

where the multiplication runs over all modes. Substituting the separable wave function *Ansatz* (eq 8) into the time-dependent Schrödinger equation (eq 1) leads to the following set of one-dimensional Schrödinger equations for the individual degrees of freedom

$$i\hbar\frac{\partial\phi_j(q_j,t)}{\partial t} = \left[-\frac{\hbar^2}{2m_j}\frac{\partial^2}{\partial {q_j}^2} + \bar{V}_j(q_j,t)\right]\phi_j(q_j,t) \tag{9}$$

where the effective single-mode potentials $\bar{V}_j$ are defined as

$$\bar{V}_j(q_j,t) = \langle\prod_{l\neq j}\phi_l(q_l,t)|V(q_1,...,q_N)|\prod_{l\neq j}\phi_l(q_l,t)\rangle + \frac{1-N}{N}\langle\prod_{l=1}^{N}\phi_l(q_l,t)|V(q_1,...,q_N)|\prod_{l=1}^{N}\phi_l(q_l,t)\rangle \tag{10}$$

The first term in eq 10 is the actual mean-field potential for mode j obtained by integrating out all the remaining degrees of freedom, while the second term is just a time-dependent energy normalization factor which defines the overall phase of the wave function. For a separable initial wave function, the TDSCF propagation as outlined above is straightforward. Provided that the wave function cannot be initially represented as a product of single-mode functions, it is, at least in principle, always possible to expand it into a series of separable terms. Employing the linearity of the Schrödinger equation, one would then propagate each term of the expansion separately.

Seemingly, the TDSCF scheme represents a perfect linearization of the multidimensional problem, replacing the N-dimensional exact propagation by N

1-dimensional approximate propagations. The reason the linearization is not complete lies in the necessity to evaluate the effective single-mode Hamiltonians. As follows from eq 10, this means performing multidimensional quadratures, which very soon becomes a bottleneck of the calculations when increasing the size of the system. Therefore, TDSCF can directly be used only for moderately large systems (say up to 10 atoms) unless the interaction potential is significantly simplified, e.g., by a low-order polynomial expansion in the normal mode coordinates. Most recently, a TDSCF scheme based on a reaction path Hamiltonian,[57] in which only the potential, gradient, and Hessian along a minimum energy path enter, has been developed.[58,59] While very useful for certain classes of potential models, the reaction path Hamiltonian method can hardly be generalized for situations with more delocalized wave functions where it is difficult to define a meaningful reaction path.

Finally, the fact that during the TDSCF calculation the propagation of each mode is performed quasi-separately does not imply that the individual degrees of freedom do not interact with each other. The approximate mean-field interactions between the modes actually follow from the form of the effective Hamiltonians which are time-dependent and depend on wave functions of all the other degrees of freedom. This time-dependence is due to the fact that the single-mode wave functions which come into the integrand in eq 10 are themselves time-dependent.

B. Multiconfigurational and Configuration Interaction TDSCF

Although in many cases, especially for fast processes with good separation of frequencies between the modes, the TDSCF methods works very well, there are well-known cases where the method is not adequate (e.g., for a particle in a double well potential coupled to an anharmonic bath[60] or for nonadiabatic processes with strong nonseparable couplings[61]). Therefore, there is clearly a need for more accurate methods that can, at least in principle, be pursued to the level of numerically exact calculations. A simple improvement of the TDSCF methods for cases where only two or a small number of modes are strongly coupled is based on an incomplete factorization of the wave function. This means that the total wave function is factorized into single-mode functions only for the weakly bound modes with the strongly bound part left unfactorized.[60,62] More sophisticated extensions of the TDSCF method approximate the exact wave function by a linear combination of product-type functions instead of a single separable wave function. This additional flexibility in the wave function *Ansatz* allows one to overcome the mean-field approximation and account for significant parts of correlation effects. The two most practical methods of this type are the multiconfiguration TDSCF (MC-TDSCF or MCTDH)[60,63−70] and the configuration interaction TDSCF (CI-TDSCF or CI-TDH).[71,72]

The simpler of the two methods, the CI-TDSCF approach, variationally optimizes the expansion coefficients $a_l(t)$ in the wave function *Ansatz*

$$\Psi(q_1,...,q_N,t) = \sum_{l=1}^{L} a_l(t)\Phi_l(q_1,...,q_N,t) \qquad (11)$$

where each of the time-dependent basis functions Φ_l is a separable wave function. For the computational scheme to be practical, the basis functions should be mutually orthogonal at all times. This is achieved by picking up at $t = 0$ an orthonormal set of functions (e.g., Hermite polynomials as eigenfunctions of the harmonic oscillator) and letting these basis functions evolve along the same TDSCF potential. For example, provided the initial wave function can be approximated by a product of Gaussians, the mean-field potential of use is that generated by time-evolving ground-state harmonic oscillator functions.

Substituting the *Ansatz* eq 11 into the time-dependent Schrödinger equation leads to the following equations for the CI coefficients $a_l(t)$

$$i\hbar\frac{\mathrm{d}a_l(t)}{\mathrm{d}t} = \sum_{m=1}^{L} a_m(t)\Xi_{lm}(t) \qquad (12)$$

The coupling coefficients $\Xi_{lm}(t)$ which correct for the error in using an approximate separable potential are defined as

$$\Xi_{lm}(t) = \langle\Phi_l(q_1,...,q_N,t)|V(q_1,...,q_N)|\Phi_m(q_1,...,q_N,t)\rangle \qquad (13)$$

where V is the (fully coupled) interaction potential.

In principle, the CI-TDSCF propagation approaches the exact solution for a complete infinite set of basis functions. From the practical point of view, a computational bottleneck of the method is its relatively slow convergence upon increasing the basis set. For large systems it is also necessary to consider that if a certain number of basis functions is required to satisfactorily describe each mode, the total number of basis functions scales exponentially with system size. Finally, a straightforward evaluation of the coupling terms in eq 13 involves N-dimensional numerical quadratures, which becomes a difficult task for systems with many degrees of freedom.

A way to speed up the convergence of the CI expansion is to allow for a full variational flexibility, i.e., to optimize using the time-dependent variational principle not only the coefficients a_l but also the basis functions Φ_l (see eq 11). This approach has been adopted in the MC-TDSCF method, several variants of which have been presented in the literature.[60,63−70] Here, we follow the elegant derivation given in refs 63 and 66, where the particular variant of the MC-TDSCF approach is systematically denoted MCTDH. The MCTDH *Ansatz* for the total wave function is as follows

$$\Psi(q_1,...,q_N,t) = \sum_{j_1}^{n_1}\cdots\sum_{j_f}^{n_N} a_{j_1\cdots j_f}(t) \times \prod_{k=1}^{N}\phi_{j_k}^{(k)}(q_k,t) \qquad (14)$$

This expression is related to the CI *Ansatz* (eq 11) except that the product form of the basis functions is now written explicitly and not only the coefficients

but also the time-dependent basis functions are optimized using the time-dependent variational principle.

It turns out that the MC-TDSCF wave function is not uniquely defined by eq 14. Therefore, to prevent redundant solutions, the following additional constraints are imposed on the single-mode wave functions

$$\langle \phi_n^{(k)}(t) | \phi_m^{(k)}(t) \rangle = \delta_{nm} \tag{15}$$

and

$$i\hbar \langle \phi_n^{(k)}(t) | \phi_m^{(k)}(t) \rangle = \langle \phi_n^{(k)}(t) | h^{(k)} | \phi_m^{(k)}(t) \rangle \tag{16}$$

Here, $h^{(k)}$ are single-mode Hamiltonians which represent the separable part of the total interaction. The full Hamiltonian is thus written as

$$H = \sum_{k=1}^{N} h^{(k)}(q_k) + U(q_1,...,q_N) \tag{17}$$

where U represents the nonseparable part of the interaction. The mean-field interactions are then defined as

$$\langle U \rangle_{nm}^{(k)} = \langle \chi_n^{(k)} | U | \chi_m^{(k)} \rangle \tag{18}$$

In the above expression for the sake of convenience we introduced wave functions $\chi_n^{(k)}$ which depend on all coordinates *except* q_k

$$\chi_n^{(k)} = \sum_{all\, j_1} \cdots \sum_{i \neq k} a_{j_1,...,j_{k-1},n,j_{k+1},...,j_N}(t) \times \prod_{l \neq k \text{bu}>} \phi_{jl}^{(l)}(q_l,t) \tag{19}$$

Using the time-dependent variational principle, from the above expressions one gets the following equations of motion for coefficients $a_J(t)$, where we use a global notation for the corresponding coefficients in eq 14

$$i\hbar \frac{\mathrm{d}a_J(t)}{\mathrm{d}t} = \sum_L \langle \Phi_J | U | \Phi_L \rangle a_L(t) \tag{20}$$

Here J and L are collective indices ($J = j_1,...,j_N$) and

$$\Phi_J = \prod_{l=1}^{N} \phi_{jl}^{(l)}(q_l) \tag{21}$$

The equations of motion which govern the time evolution of the single-mode wave function are as follows

$$i\hbar \frac{\partial \phi^{(k)}}{\partial t} = h^{(k)}\phi^{(k)} + [1 - P^{(k)}]\rho^{(k)-1}\langle \mathbf{U} \rangle^{(k)}\phi^{(k)} \tag{22}$$

Here, $\phi^{(k)}$ is a vector of single-mode wave functions, $\rho^{(k)}$ is a density matrix constructed from the wave function $\chi_n^{(k)}$ of eq 18, and $P^{(k)}$ is a time-dependent projection on the space spanned by the single-mode wave functions $\phi_j^{(k)}$. $\langle U \rangle^{(k)}$ are the matrix representations of the mean-field interactions defined in eq 18. The MC-TDSCF equations of motion thus consist of propagation of the coefficients of configurations (see eq 20) together with the single-mode basis functions (see eq 22). The MC-TDSCF method can be of very high accuracy and generally exhibits a fast convergence with respect to the size of the basis set. Nevertheless, the number of necessary basis functions grows exponentially with the system size and the method becomes computationally very demanding for larger systems.

C. Classical Separable Potential Method and Its Configuration Interaction Extension

The TDSCF method as a significant simplification of the numerically exact propagation of the time-dependent Schrödinger equation represents an important step forward toward practical quantum simulations of large polyatomic systems. Nevertheless, it leaves us with the necessity to evaluate the effective single-mode Hamiltonians via multidimensional numerical quadratures (see eq 10). In some cases, it is possible to split the polyatomic system into classical and quantum parts and treat only the smaller quantum part using the TDSCF method.[73] In other cases, it is plausible to assume a special simple form of the interaction potential which leads to one-dimensional quadratures.[74] In this section, we pursue a more general approach which works for any type of interactions and generates a separable wave function for the whole polyatomic system.

The basic idea behind the recently developed classical separable potential (CSP) method[49,75] is to approximate the numerically extremely demanding multidimensional integrals over TDSCF wave functions by weighted averages over properly selected classical trajectories. This is a practical way to overcome the computational bottleneck of the TDSCF method, allowing for quantum simulations of systems with hundreds to thousands of degrees of freedom. The CSP method has proven to work very well for fast processes in moderately quantal systems[76−78] and gives results in quantitative agreement with TDSCF propagations in cases where the latter calculations are feasible.[75,79] The principle reason for this is that the classical approximation is used only for the evaluation of mean-field interactions, and for such average quantities, the classical approximation is very accurate. Moreover, in the expression for the TDSCF Hamiltonians (see eq 10), only real wave function amplitudes and no complex phases show up. While it is very difficult to reproduce quantum phase relations using classical propagations, already a small number of trajectories can very well mimic the square of the wave function, i.e., the quantum probability function. Thus, within the CSP method, all the single-mode quantum effects are exactly preserved and approximations are introduced only for interactions between the modes.

The CSP scheme consists of the following four steps: (i) Mapping the initial wave function onto a set of classical coordinates and momenta, (ii) propagation of a set of classical trajectories, (iii) construction of the time-dependent CSP potentials, and (iv) quantum one-dimensional propagations for each mode using the CSP potentials.

Let us elaborate in more detail on these steps. Since the classical trajectories should mimic the quantum evolution as well as possible, their initial conditions should correspond to the initial quantum wave function. This is accomplished by mapping the initial wave function $\Psi(\vec{q},0)$ onto a weighted set $P_w(\vec{q},\vec{q})$ of initial coordinates and momenta using the Wigner distribution[80,81]

$$P_w(\vec{q},\vec{q}) = \frac{1}{\pi\hbar}\int_{-\infty}^{\infty} d\vec{y}\,\Psi^*(\vec{q}+\vec{y},0)\Psi(\vec{q}-\vec{y},0)e^{2i\vec{p}\vec{y}/\hbar} \quad (23)$$

For separable initial wave functions, the expression in eq 23 breaks into a product of one-dimensional integrals. If the initial wave function is a Gaussian, the integral can be evaluated analytically and the resulting Wigner distribution is also Gaussian.

Once the initial coordinates, momenta, and weights are generated, a swarm of classical trajectories is propagated by numerically solving the Newton equations of motion in a standard way.[17] The number of trajectories needed for providing converged effective potentials depends on the particular process under study, the size of the system, the initial wave function, and the duration of the simulation. Typically, 100−1000 trajectories are necessary for systems with tens to hundreds of atoms, which represents a relatively simple computational task.

Once the classical trajectories are generated, a time-dependent classical separable potential $\bar{V}^{CSP}$ is evaluated for each mode j

$$\bar{V}_j^{CSP}(q_j,t) = \sum_{\alpha=1}^{n_T} V(q_1^{(\alpha)}(t),...,q^{j-1(\alpha)}(t),q_j,q_{j+1}^{(\alpha)}(t),...,q_N^{(\alpha)}(t))\omega_\alpha + \frac{1-N}{N}\bar{V}(t) \quad (24)$$

where $V(q_1,...,q_N)$ is the full potential function of the system, $\omega_\alpha = P_w(\vec{q}^\alpha,\vec{p}^\alpha)$ is the Wigner weight of the α trajectory in the initial state distribution, and the summation in eq 24 extends over all MD trajectories. The time-dependent energy normalization factor $\bar{V}(t)$ is given as

$$\bar{V}(t) = \sum_{\alpha=1}^{n_T} V(q_1^{(\alpha)}(t),...,q_j^{(\alpha)}(t),...,q_N^{(\alpha)}(t))\omega_\alpha \quad (25)$$

Note the analogy between the definition of the TDSCF potentials in eq 10 and the above CSP potentials, where numerically tedious multidimensional integrations are replaced by (weighted) summations over classical trajectories. This gives the CSP method an enormous computational advantage and makes it a truly practical method for large systems.

Finally, the time-dependent Schrödinger equation

$$i\hbar\frac{\partial\phi_j(q_j,t)}{\partial t} = [T_j + \bar{V}_j^{CSP}(q_j,t)]\phi_j(q_j,t) \quad (26)$$

is numerically solved for each mode j. The total CSP wave function is then given in a product form as

$$\psi(q_1,...,q_N,t) = \prod_{j=1}^{N}\phi_j(q_j,t) \quad (27)$$

From a computational point of view, it is important to mention that due to the use of classical trajectories to evaluate the time-dependent single-mode potentials, the quantum CSP energy, unlike the total TDSCF energy which is obtained self-consistently, is not strictly conserved. Significant fluctuations or a drift in time of the total CSP energy would indicate that the classical trajectories cease to faithfully represent the quantum wave function and the validity of the approximation would come under question. In most cases, the extent of the nonconservation is, however, small and does not seem to create significant difficulties.

The CSP method basically involves two different kinds of approximations—one following from the separable nature of the quantum wave function, the other being connected with use of classical trajectories for the construction of effective single-mode potentials. In the test cases studied so far,[75,79] classical separable potentials are practically identical to the TDSCF mean-field potentials and for moderately quantal systems we do not expect large deviations from this behavior. On the other hand, it is well-recognized that the accuracy of separable methods decays rapidly in time due to cumulative errors resulting from the difference between mean-field and exact couplings between the modes. Therefore, there is a clear need to extend the CSP method beyond the separable approximation.

As in the case of the TDSCF approach, the extensions go in the direction of replacing a separable wave function *Ansatz* by a linear combination of product terms. A very simple, nonvariational extension of the CSP method does not propagate a single separable wave function along the potential averaged over all trajectories but rather generates one separable wave function $\Psi^{(\alpha)} = \prod_{j=1}^{N}\phi_j^{(\alpha)}(q_j,t)$ along each trajectory α, i.e., subject to a potential $V_j^{(\alpha)}$ defined as

$$V_j^{(\alpha)}(q_j,t) = V(q_1^{(\alpha)}(t),...,q_{j-1}^{(\alpha)}(t),q_j,q_{j+1}^{(\alpha)}(t),...,q_N^{(\alpha)}(t)) + \frac{1-N}{N}\bar{V}^{(\alpha)}(t) \quad (28)$$

The coordinate-independent constants $\bar{V}^{(\alpha)}$

$$\bar{V}^{(\alpha)}(t) = V(q_1^{(\alpha)}(t),...,q_j^{(\alpha)}(t),...,q_N^{(\alpha)}(t)) \quad (29)$$

again do not influence the dynamics and are only added for energy normalization.

In this scheme, named post-averaging CSP in ref 77, the expectation value of any operator $\hat{A}_k$ corresponding to an observable for mode k (e.g., position, kinetic energy, etc.) is evaluated as

$$\langle A_k\rangle = \sum_{\alpha=1}^{n_T}\omega_\alpha\,\langle\phi_k^{(\alpha)}(q_k,t)|\hat{A}_k|\phi_k^{(\alpha)}(q_k,t)\rangle \quad (30)$$

where ω_α is again the Wigner weight of trajectory α. Despite the simplicity of this scheme, it has proven

to be a significant improvement over the CSP method in accounting for interactions between the modes.[82] It is, however, clear that a method guided by a limited number of trajectories may have problems to account for rare events, especially if the trajectories spread significantly resulting in a sparse sampling of the phase space.

In the following, we outline a more elaborate configuration interaction extension of the CSP method (CI−CSP) where the CI coefficients are allowed to evolve in time.[79,83] To overcome the unfavorable scaling of CI methods with the system size, classical trajectories, which describe a fully correlated dynamics, are used to guide the selection of important CI terms and to enable evaluation of coupling terms without multidimensional quadratures. The CI method is based on the time-dependent variational principle which ensures superiority of the CI results to the CSP ones. The degree of improvement over the separable CSP method crucially depends on the right choice of the CI terms. Here, one relies on the fact that classical mechanics are fully correlated and that moderately quantal systems modes that are strongly correlated classically will also exhibit this property in quantum mechanics.

The CI−CSP method starts with propagating separable wave functions $\Psi(\alpha)$ along individual trajectories exactly as in the post-averaging CSP scheme (see eqs 28 and 29) together with the CSP wave function guided by the CSP potential (see eqs 24−27).

In the current formulation, the CI−CSP *Ansatz* to the wave function allows for explicit couplings between pairs of modes

$$\Psi^{CI-CSP}(q_1,...,q_N,t) = c_0(t)\phi_1{}^0(q_1,t)...\phi_N{}^0(q_N,t) + \sum_{j,\alpha}^{N,M_j} s_{j\alpha}(t)\phi_1{}^0(q_1,t)...\phi_j{}^{(\alpha)}(q_j,t)...\phi_N{}^0(q_N,t) + \sum_{j(<j'),\alpha,j',\beta}^{N,M_j,N,M_{j'}} d_{j\alpha j'\beta}(t)\phi_1{}^0(q_1,t)...\phi_j{}^{(\alpha)}(q_j,t)...\phi_j{}^{(\beta)}(q_{j'},t)... \phi_N{}^0(q_N,t) \quad (31)$$

Here, $\phi_j{}^0$ are the CSP functions and symbols $\phi_j{}^{(\alpha)}$ denote j-mode wave functions propagated along trajectory α. New terms are included into the CI space when the overlap between $\phi_j{}^0$ and $\phi_j{}^{(\alpha)}$ drops below a certain threshold (typically 0.95). In this way, the CI space is steadily growing and thus accommodates the evolution of correlations between the modes. To make the CI problem computationally tractable, the wave functions $\phi_j{}^{(\alpha)}$ are orthogonalized with respect to the CSP wave functions and each other using the standard Schmidt orthogonalization procedure. Finally, $c_0(t)$ is the CSP coefficient, $s_{j\alpha}(t)$ stands in front of single-mode "polarization" terms, and $d_{j\alpha j'\beta}(t)$ are terms standing in front of two-mode correlation terms, higher order correlations being neglected. The working CI−CSP equations are obtained by implementing the wave function *Ansatz* from eq 31 into the time-dependent Schrödinger equation. The full set of equations is rather complicated and has been presented as an Appendix to ref 83. Here, we show a simplified set of equations obtained by assuming a separable initial wave function and by taking into account only the leading coupling terms, namely, couplings between the CSP and the two-mode correlated terms (neglecting all the single-mode polarization terms)[79,83]

$$i\hbar\frac{\partial c_0}{\partial t} = \sum_{j(<j'),\alpha,i',\beta}^{N,M_j,N,M_{j'}} d_{j\alpha j'}\beta\,\langle\psi_j{}^0\psi_{j'}{}^0|V_{jj'}{}^{CSP2}|\psi_j{}^{(\alpha)}\psi_{j'}{}^{(\beta)}\rangle \quad (32)$$

$$i\hbar\frac{\partial d_{j\alpha j'\beta}}{\partial t} = c_0\,\langle\psi_j{}^{(\alpha)}\psi_{j'}{}^{(\beta)}|V_{jj'}{}^{CSP2}|\psi_j{}^0\psi_{j'}{}^0\rangle \quad (33)$$

Here, the 2-dimensional CSP-like potentials $V_{jj'}{}^{CSP2}$ are given as

$$V_{jj'}{}^{CSP2}(q_j,q_{j'},t) = \sum_{\alpha=1}^{n_T} V(q_1{}^{(\alpha)}(t),...,q_j,...,q_{j'},...,q_N{}^{(\alpha)}(t))\omega_\alpha \quad (34)$$

where the summation runs over all trajectories. Thus, the CI−CSP method explicitly accounts for correlations between pairs of modes which are the major terms missed by the separable CSP approach. Due to the guidance of classical mechanics, only the important terms are included and the number of CI functions providing converged results at this level is relatively modest (typically few thousands).[83] CI−CSP calculation can therefore be pursued for large systems, although the computational cost is significantly higher than that of the CSP propagation.

D. Gaussian-Based Semiclassical Methods

The approximate quantum dynamical methods introduced in previous subsections involve different kinds of approximations concerning the form of the wave function or the way the effective potentials are evaluated. The propagation in time remains, however, fully on the quantum mechanical footing. In this subsection, we introduce methods which are based on semiclassical approximations to the quantum propagator itself. Since this extensive field of research has already been reviewed in great detail,[84,85] we concentrate only on the basic concepts and on presenting the most recent approaches not covered by refs 84 and 85.

The time-dependent quantum mechanical propagator is defined as[86,87]

$$K(\vec{x}',\vec{x},t) = \langle\vec{x}'|e^{-(i/\hbar)\hat{H}t}|\vec{x}\rangle \quad (35)$$

and satisfies the time-dependent Schrödinger equation

$$i\hbar\frac{\partial K(\vec{x}',\vec{x},t)}{\partial t} = \hat{H}(\vec{x}')K(\vec{x}',\vec{x},t) \quad (36)$$

with an initial condition

$$K(\vec{x}',\vec{x},0) = \delta(\vec{x}' - \vec{x}) \quad (37)$$

The wave function is then propagated as

$$\Psi(\vec{x}',t) = \int d\vec{x}K(\vec{x}',\vec{x},t)\Psi(\vec{x},0) \quad (38)$$

Methods described here replace the exact quantum propagator by a semiclassical approximation. Following Van Vleck by solving eq 36 asymptotically to the order of $O(\hbar)$ or applying a stationary phase treatment to the path integral expression to K gives a semiclassical propagator[86−89]

$$K^{SC}(\vec{x}',\vec{x},t) = (2\pi i\hbar)^{n/2} \sum_{traj} \frac{e^{(i/\hbar)S(\vec{x}',\vec{x},t)} e^{-(i/2)\pi\nu}}{|det\left(\frac{\partial \vec{x}'}{\partial \vec{p}}\right)|^{1/2}} \quad (39)$$

where n is the number of degrees of freedom, ν is the Maslov index, the summation extends over all classical trajectories connecting point $\vec{x}$ at time 0 to point $\vec{x}'$ at time t, and $S(\vec{x}',\vec{x},t)$ is the classical action along such a trajectory.

Putting aside problems arising when the semiclassical propagator in eq 39 becomes singular at caustics, a major drawback for application lies in the fact that the propagator is in the boundary representation rather than in the initial value representation. It is practically impossible to generate all trajectories connecting the points $(\vec{x},0)$ and $(\vec{x}',t)$ for any realistic polyatomic system. Therefore, computationally efficient semiclassical schemes start with reformulating eq 39 into an initial value problem where trajectories are simply run forward in time from a set of initial conditions such as in standard MD simulations. This is done by replacing the semiclassical propagation by a function of both coordinates and momenta. In the limit $\hbar \rightarrow 0$, this leads to[86,87]

$$K^{SC}(\vec{x}',\vec{x}) = \int d\vec{p} \int d\vec{q} M_{\vec{p}\vec{q}}(\vec{x}',\vec{x},t) \quad (40)$$

where the function M depends on coordinates $\vec{q}_t$ and momenta $\vec{p}_t$ that are obtained by propagating classical trajectories starting from initial conditions $(\vec{p},\vec{p})$. The particular choice of function M is not unique and leads to different semiclassical propagation methods. One particular choice leads to the so-called cellular dynamics method,[90] while other choices are equivalent to the earlier developed schemes by Herman and Kluk[91,92] or Heller.[93−95]

In the context of the initial value semiclassical propagation, one should at least briefly mention the issue of degradation of the method in the presence of chaotic trajectories. Clearly, propagators based on classical trajectories give rise to computational difficulties in the chaotic regime, where an infinitesimal change in the initial conditions results in a drastically different long time behavior. At least for small model systems, this problem has been recently successfully handled using the integral conditioning technique for preaveraging the phase space integral over frozen Gaussians.[96] Possible future applications to large systems require further methodological and algorithmic attention.

It is illuminating to follow at least briefly different pathways of the development of the semiclassical theory. Pechukas has provided a dynamically consistent formulation of the coupling between classical and quantum degrees of freedom[97] based on the path−integral formalism.[98] This approach does not involve any further approximation beyond the semiclassical Van Vleck propagator; however, it requires propagation of complex-valued trajectories corresponding to classically forbidden processes,[99] which makes it computationally rather impractical.

Another way of deriving the semiclassical propagation, from which it most naturally follows why Gaussian wave packets are so omnipresent in semiclassical theories, has been used by Heller.[93] The starting point is a direct consequence of the Ehrenfest theorem,[100] namely, that in harmonic potentials Gaussian wave packets remain Gaussian and expectation values of positions and momenta follow classical equations of motions. A general Gaussian wave packet can be written as

$$\phi(x,t) = e^{(i/\hbar)[\alpha_t(x-x_t)^2 + p_t(x-x_t)+\gamma_t]} \quad (41)$$

where x_t and p_t are real time-dependent parameters while α_t and γ_t are complex. Assuming a locally quadratic Hamiltonian around the center x_t of the time-dependent Gaussian

$$H \approx -\frac{\hbar^2}{2m}\frac{\partial^2}{\partial x^2} + V(x_t) + \frac{\partial V(x)}{\partial x}|_{x=x_t}(x - x_t) + \frac{1}{2}\frac{\partial^2 V(x)}{\partial x^2}|_{x=x_t}(x - x_t)^2 \quad (42)$$

simplifies the time-dependent Schrödinger equation to the following set of equations for the parameters of the Gaussian functions[93]

$$\frac{\partial x_t}{\partial t} = \frac{\partial H}{\partial p_t} \quad (43)$$

$$\frac{\partial p_t}{\partial t} = -\frac{\partial H}{\partial x_t} \quad (44)$$

$$\frac{\partial \alpha_t}{\partial t} = -\frac{2}{m}\alpha_t^2 - \frac{1}{2}\frac{\partial^2 V(x)}{\partial x^2}|_{x=x_t} \quad (45)$$

$$\frac{\partial \gamma_t}{\partial t} = i\hbar\frac{\alpha_t}{m} + p_t\frac{\partial x_t}{\partial t} - \frac{p_t^2}{2m} - V(x_t) \quad (46)$$

We immediately see that the center of the Gaussian wave packet and the center of its momentum evolve according to classical Hamiltonian equations of motion, while the width parameter α and the phase γ do not have a classical analogue. On one hand, the quasiclassical motion of the Gaussians provides a lot of intuitive insight; on the other hand, it effectively prevents the description of deeply quantal effects such as tunneling.

Several methods have been developed recently which dwell on the semiclassical ideas presented above with the purpose of obtaining practical computational schemes for large polyatomic systems. The so-called cellularized frozen Gaussian approximation[101,102] which combines the most attractive features of the frozen Gaussian approximation[91,92] and the cellular dynamics algorithm[90] has been applied to systems with up to 15 degrees of freedom. A different approach,[103−105] which allows for simulations of hun-

dreds of atoms, starts with dividing modes according to their thermal occupation. Subsequently, only the more quantal degrees of freedom with low thermal occupancy are treated more rigorously by the Van Vleck propagator which involves a second-order approximation in stationary phase.[88] The rest of the system is treated in a zeroth-order approximation by simply propagating classical trajectories weighted by the action accumulated along the classical path.

The last two methods discussed in this subsection have been tailored to nonadiabatic molecular processes. Leaving aside various schemes based either on the surface-hopping[106−112] or classical path[113−115] approaches which couple dynamically nuclear and electronic degrees of freedom treating the nuclear modes classically, we concentrate here on newly developed approximate nonadiabatic quantum dynamical methods. First we note, however, that the surface-hopping method has been very recently extended toward a semiclassical description of nuclear motions,[116−118] and the same is true also for the classical path approach.[119] These approaches are also promising for large systems provided the motions are relatively localized and the underlying potentials and nonadiabatic couplings are not too complex.

Within the multiple spawning method,[120−126] the time-dependent nuclear wave function $\Psi_I(\vec{x},t)$ associated with each electronic state I is expanded into a series of multidimensional traveling Gaussian basis functions with time-dependent weights

$$\Psi_I(\vec{x},t) = \sum_j d_{Ij}(t)\chi_{Ij}(\vec{R};\vec{R}_{Ij}(t),\vec{P}_{Ij}(t),\gamma_{Ij}(t),\alpha_{Ij}) \quad (47)$$

The connection to classical mechanics is made by letting the centers R_{Ij} and centers of momentum P_{Ij} of the Gaussians follow classical equations of motion. The Gaussian widths α_{Ij} are fixed, and the equation governing the time evolution of the phase factors γ_{Ij} is that obtained in the local harmonic approximation (see eq 46). Since the Gaussian basis set is nonorthogonal, excessive linear dependence has to be prevented by regularization of the overlap matrix to avoid numerical problems. To keep the size of the basis set under control, a spawning procedure is applied where basis functions are gradually added to an initial modest set whenever needed, namely, in the regions of nonadiabatic events.

The basic idea behind the mapping formalism approach[127,128] to nonadiabatic dynamics is to map discrete electronic states onto continuous variables, bringing them on the same footing as the nuclear degrees of freedom. Let the N-electronic-level system be described by a Hamiltonian

$$\hat{H} = \sum_{n,m} h_{nm}|\phi_n\rangle\langle\phi_m| \quad (48)$$

The electronic states are then mapped onto a set of harmonic oscillator basis states

$$|\phi_n\rangle \rightarrow |0_1....1_n....0_N\rangle \quad (49)$$

$$|\phi_n\rangle\langle\phi_m| \rightarrow a_n^+ a_m \quad (50)$$

where a_m and a_n^+ are the harmonic oscillator creation and annihilation operators. Introducing the electronic variables $X_n = (a_n^+ + a_m)/\sqrt{2}$, $P_n = i(a_n^+ - a_m)/\sqrt{2}$ and the electronic occupation operator $N_n = 1/2(X_n^2 + P_n^2 - 1)$ leads to the following form of the mapped Hamiltonian of the coupled electronic and nuclear system

$$\hat{H} = \hat{T} + \sum_n N_n V_{nn}(\vec{x}) + \sum_{n>m}(X_n X_m + P_n P_m)V_{nm}(\vec{x}) \quad (51)$$

Here, the first two terms correspond to adiabatic dynamics on particular electronic surfaces while the last term represents the nonadiabatic couplings. The principal advantage of the mapping algorithm is that the Hamiltonian in eq 51 has a clear classical analogue. Therefore, one can straightforwardly apply a semiclassical representation[91] as in the case of adiabatic dynamics on a single electronic surface. Finally, we note that similar ideas concerning mapping onto angular momenta rather than harmonic oscillators were already introduced 20 years ago, however, purely within the framework of classical mechanics.[129]

Undoubtedly, Gaussian-based semiclassical approximations at their simpler levels represent very useful tools for dealing with moderate quantum effects both in small and large systems. To the present authors it seems that, at least in the current state, it is not clear that the more complex algorithms, which provide greater accuracy and better description of quantum effects, can be directly applied to large systems. For atom-scale masses, the physical basis for semiclassical treatments is compelling and evidence from applications to simple models suggests that high accuracy and fine details can be obtained. The problem is with the computational efficiency which is often comparable with that of the numerically exact quantum propagation. However, several studies indicate that in the future it might be possible to overcome some of the numerical difficulties connected with semiclassical propagations. For example, most recently a computationally simple linearized approximation to the semiclassical initial value representation has been developed and applied to reactive flux calculations both on a single and on multiple electronic surfaces.[130,131]

E. Dynamic Path Integral Methods

We discuss in this subsection applications of the Feynman path integral formalism[98] to quantum molecular dynamics. As a matter of fact, path integral formulation of quantum mechanics has been extremely important for deriving the semiclassical approximations discussed above. However, until recently, numerical applications have been restricted to propagations in imaginary time using Monte Carlo sampling techniques providing equilibrium thermodynamic properties. This is due to the fact that the real time propagator is highly oscillatory and standard Monte Carlo schemes fail.

Several recent approaches deal with problems connected with real time propagations in ways that lead to computationally efficient methods. Several

schemes, targeted primarily at evaluation of time correlation functions, are based on analytical continuation of imaginary time quantities[132] or on combining real and imaginary time quantum Monte Carlo data[133] via the maximum entropy method. Within the former method, correlation functions are calculated in imaginary time by standard equilibrium quantum Monte Carlo. An analytical continuation procedure is then applied in order to obtain the desired real time correlation functions. The main problem is that the analytical continuation method is numerically unstable and numerical errors get magnified in an uncontrollable way during the simulation, which is an issue addressed by several researches.[134] The latter method deals with this numerical instability by applying the maximum entropy method for inverting the imaginary time functions into real time data. Numerically, the most efficient procedures are based on a combination of imaginary and real time data.[133] Finally, for the special case of spin-boson systems, a real time quantum Monte Carlo approach which removes the numerical instabilities by a Hubbard−Stratonovich transformation of the path integral has been recently developed.[135,136]

For processes with a good system−bath separation, the quasi-adiabatic propagator path integral method[137−139] works very well and allows for simulations of processes in very large systems such as the charge-transfer in the photosynthetic reaction center.[140] Within this approach a smoothly converging propagator is constructed which incorporates the exact dynamics of a physically motivated reference system (e.g., isolated system without the bath). In this way, the oscillation or sign problems, which are fundamental manifestations of quantum mechanics, can be handled numerically. In practical applications, the coupled many-body Hamiltonian is partitioned into a reference part H_{ref} and an interaction term $H_{\mathrm{int}} = H - H_{\mathrm{ref}}$ which contains nonseparable interactions. The uncoupled reference problem is solved by a combination of analytical and numerical techniques and the short-time evolution operator $\hat{U}$ is then approximately split in the following way

$$\hat{U}(\delta t) = e^{-(i/\hbar)\hat{H}\delta t} \approx e^{-(i/2\hbar)\hat{H}_{\mathrm{int}}\delta t}\, e^{-(i/\hbar)\hat{H}_{\mathrm{ref}}\delta t}\, e^{-(i/2\hbar)\hat{H}_{\mathrm{int}}\delta t} \tag{52}$$

The path integral formulation is then obtained as the coordinate representation of the above propagator

$$\langle \vec{x}_k | e^{-(i/\hbar)\hat{H}\delta t} | \vec{x}_{k-1} \rangle \approx \langle \vec{x}_k | e^{-(i/\hbar)\hat{H}_{\mathrm{ref}}\delta t} | \vec{x}_{k-1} \rangle\, e^{-(i/2\hbar)\delta t[\hat{H}_{\mathrm{int}}(\vec{x}_k)+\hat{H}_{\mathrm{int}}(\vec{x}_{k-1})]} \tag{53}$$

A physically meaningful choice of the reference Hamiltonian leads to an accurate propagator for which large time steps can be used. A necessary condition is clearly the knowledge of the reference propagator which requires simple reference Hamiltonians such as the separable part of the total Hamiltonian.

The centroid molecular dynamics method[141−145] takes a different route by focusing on an ensemble-averaged time evolution of a quantum system. In this method, which becomes exact for quadratic potentials, the so-called system centroids evolve classically on a potential of mean force created by averaging over all quantum fluctuations of the imaginary time Feynman path integral at fixed path centroid positions. The centroid dynamics is thus inherently semiclassical, with computational advantages specific to this approach. The equation of motion of the system path centroids is then

$$m\frac{\mathrm{d}^2\vec{x}_c(t)}{\mathrm{d}t^2} = -\nabla_c V_c(\vec{x}_c) \tag{54}$$

where the left-hand side of the equation represents the force on the centroids and $\vec{x}_c$ is a set of coordinates of all centroids of the system. The centroid potential of mean-field V_c is given as

$$V_c(\vec{x}_c) = -k_{\mathrm{B}}T \ln(\rho_c(\vec{x}_c)/\rho_c{}^0) \tag{55}$$

where $\rho_c{}^0$ is the free particle centroid density and $\rho_c(\vec{x}_c)$ is given by a constrained path integral. By numerical discretization, a path integral is obtained which looks like a classical configurational integral over an extended configuration space. While several interesting applications of the method have been presented, detailed analysis of its accuracy and validity range for realistic systems has not been carried out yet.

V. Applications

Despite large efforts directed toward development of quantum dynamical methods, the number of applications to realistic, experimentally relevant large polyatomic systems is rather modest, especially if compared to the vast amount of classical MD studies. Nevertheless, there has been a lot of progress recently and quantum molecular dynamics has been applied to areas ranging from atom−cluster scattering over photophysics and photochemistry of chromophores embedded in clusters or matrixes and of large molecules, to hydrogen diffusion in crystals, primary processes in photosynthesis, and the process of vision. In general, quantum simulations have proven to be useful tools for studying ultrafast processes in polyatomics, as probed mainly by frequency-domain or real-time pump−probe spectroscopy. In the next subsections, we review several representative applications roughly following the order of methods presented in the previous section.

A. Helium Scattering from Large Argon and Water Clusters

Scattering of a light atom from cryogenic clusters has proven to be a very useful method for studying the vibrational structure and excitations of clusters. For small clusters, discrete molecular vibrations are observed, while very large clusters approach the continuous phonon dispersion curves of corresponding solids. The low-energy modes are especially crucial for determining the structural, thermodynamic, and dynamic behavior of clusters. The most interesting questions which arise and are addressed both by experiment and theory are as follows: Which

modes get excited by the collision process? Is the excitation of a single-phonon or multiphonon character? Is there a difference in the excitation pattern between surface and bulk modes? Is the outcome of the process determined primarily by the direct collision event or also by a subsequent intracluster vibrational dynamics?

The scattering experiments have been performed in a crossed molecular beam arrangement. Low-energy helium atoms have been scattered from argon clusters with average sizes ranging from 23 to 4600 atoms or from water clusters with an average size of 110 atoms generated by adiabatic expansions with conical nozzles.[146−149] The time-of-flight spectra of the helium atom for different scattering angles have been recorded and transferred into energy-loss spectra. For the argon clusters, the principal experimental results are as follows. Only single-phonon excitations are seen for small scattering angles, while for larger scattering angles corresponding to more direct collisions, multiphonon excitations are also observed. The size dependence of the energy transfer is well-reproduced for large clusters by a simple model of a vibrating homogeneous sphere, especially for the collective surface breathing mode. The situation in water clusters is much more complicated due to the richer variety of vibrational and rotational excitations. Still, the time-of-flight spectra can be rationalized in terms of single-phonon and multiphonon excitations.

Quantum TDSCF simulations have been performed for helium scattering from a "magic number" Ar_{13} system[49,150] which is somewhat smaller than the experimentally produced clusters. In the calculations, the argon cluster has been treated quantum mechanically within its normal mode framework while the helium atom has been described classically. The TDSCF calculations are made practical by expanding the interaction Hamiltonian in the cluster normal modes and treating explicitly only the diagonal and two-mode terms. The vibrational excitation of the cluster is, in accord with experimental observations, strongly mode-selective, and despite the size of the system, even the final vibrational state distribution is not statistical. This is demonstrated in Figure 1 which shows the vibrational energy distribution versus the mode number for a head-on $He-Ar_{13}$ collision. The most strongly excited mode no. 13 represents a kind of surface vibration which couples very well with the incoming helium atom.

Helium scattering from a larger Ar_{55} cluster has been simulated on the quantum mechanical level using the vibrationally sudden approximation[151] within a harmonic treatment of cluster vibrations. In the sudden approximation it is assumed that the effective scattering time is short compared to cluster vibrational periods; therefore, the cluster is assumed to be frozen during the collision. As shown in Figure 2, such calculations reproduce the experimental time-of-flight spectra for the whole range of scattering angles very well. It should be stressed at this point that for smaller scattering angles corresponding to single-photon excitations, purely classical calculations are unable to reach satisfactory accord with experiment and quantum effects must be taken into account.

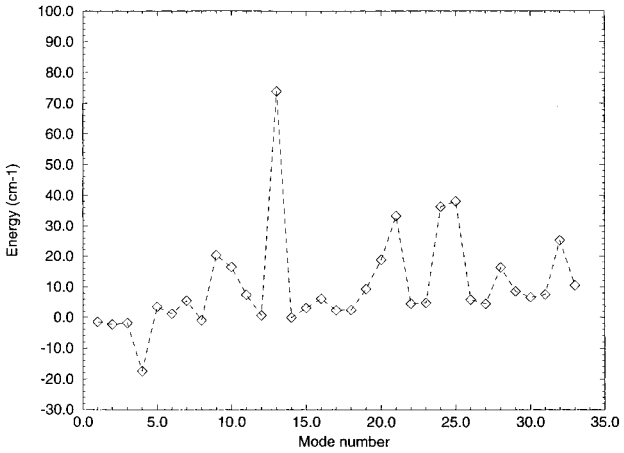

Figure 1. Vibrational energy distribution versus the mode number for a $He-Ar_{13}$ collision with zero impact parameter. (Reprinted with permission from ref 150. Copyright 1997 American Institute of Physics.)

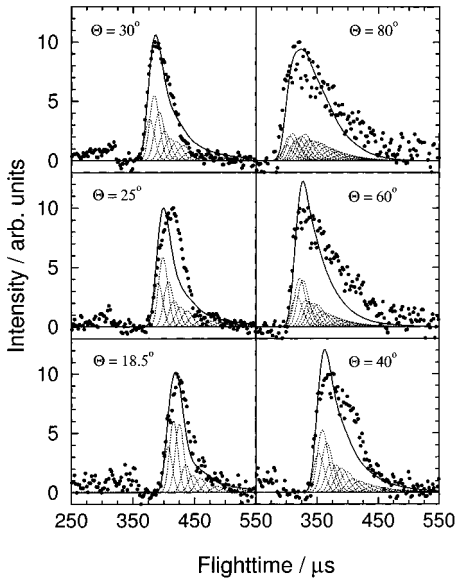

Figure 2. Comparison of experimental (●) and calculated (—) time-of-flight spectra for inelastic transitions for intermediate scattering angles in $He + Ar_{55}$ collisions. The dotted curves are the individual contributions convoluted with the experimental resolution of 0.8 meV. (Reprinted with permission from ref 151. Copyright 1997 American Institute of Physics.)

Water clusters scattering both by helium and argon atoms has been modeled.[49,149,152−153] Calculations for helium scattering from a $(H_2O)_{90}$ cluster[149] employ a method similar to the forced oscillator model, treating the quantum cluster modes harmonically and the incident atom classically. They allow for rationalizing the three observed peaks in the time-of-flight spectra[149] in terms of elastic scattering, collective cluster excitations, and water monomer rotations. Calculations of cluster mode excitations also show that peaks corresponding to surface water molecules are slightly shifted from those of the inner waters.

TDSCF calculations of argon scattering from the $(H_2O)_{11}$ cluster[152] indicate again the importance of quantum effects in the excitation of the cluster.

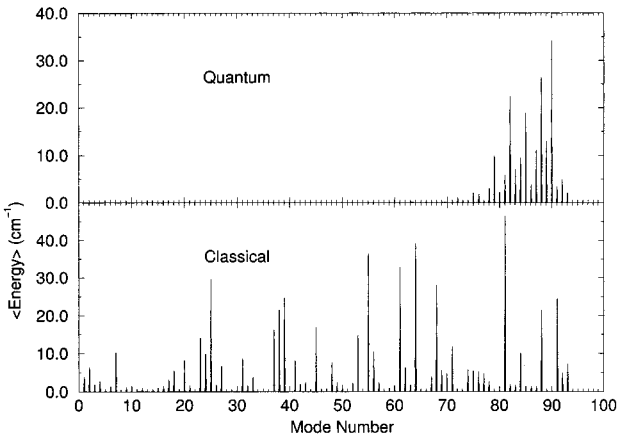

Figure 3. Mean excitation energy for each mode in Ar + $(H_2O)_{11}$ collisions. Quantum and classical results are compared. (Reprinted with permission from ref 152. Copyright 1998 American Institute of Physics.)

Figure 3 compares quantum TDSCF to classical excitations of water modes. It can immediately be seen that due to the nonconservation of the zero-point energy, classical calculations wrongly predict efficient excitation of many stiffer modes, most of which being quantum mechanically forbidden. There are also discrepancies in the soft modes, which is due to the fact that the scattered atom dominantly excites a single-mode which, unlike multiphonon excitations, is a highly nonclassical process.

Very recently, quantum TDSCF simulations have also been carried out for the He + $(H_2O)_{11}$ system, together with crossed molecular beam scattering experiments.[153] Apart from direct comparison with experimental time-of-flight data, quantum calculations also provide a direct physical interpretation of the process. The main findings are that most of the energy transfer takes place in single-quantum transitions, mostly shearing modes within a single ring or delocalized over two adjacent rings (the $(H_2O)_{11}$ cluster has a structure of interlocking rings) are excited, finally, in the experimental energy range the scattering is almost entirely direct and practically no resonances are observed, which is different from the case of argon scattering.

B. Spectroscopy and Quantum Dynamics of Photoexcited Pyrazine

Pyrazine represents one of the few aromatic molecules for which spectroscopy not only of the first excited singlet state S_1 but also of the second excited singlet S_2 is well-established. Experimentally, the absorption spectrum of this molecule has been accurately determined.[154] It has been observed that excitation to the S_1 state gives a set of discrete lines, while excitation to the S_2 state results in a broad band with a weak vibrational structure. Since there is a conical intersection between the S_1 and S_2 surfaces, this observation indicates that there is a fast $S_2 \rightarrow S_1$ internal conversion process in pyrazine.

From a theoretical point of view, the pyrazine molecule has served as a model system on which various methods have been tested and shaped. Since the process under study is very fast (depletion of the S_2 state takes only several hundreds of femtoseconds), the time-dependent quantum methodology turns out to be appropriate and useful for modeling the experimental absorption spectra and understanding the underlying dynamics. Namely, the autocorrelation function $C(t)$ which is the complex overlap between the initial wave function and the wave function at time t can be converted into the absorption spectrum[155] via a Fourier transform

$$I(\omega) \approx \omega \int_{-\infty}^{\infty} C(t) e^{i(E_i+\hbar\omega)t}\, dt \qquad (56)$$

Here, I is the absorption intensity at frequency ω and E_i is the initial energy.

The problem of the decay of the population of the S_2 state after photoexcitation due to coupling to the S_1 surface has been addressed by a semiclassical TDSCF method which combines a Gaussian wave packet *Ansatz* for the vibrational modes with a mean-field coupling between nuclear and electronic degrees of freedom.[156] Despite the fact that these approximations are rather crude, the resulting populations should be quite reliable. This is supported by comparison to exact calculations for a simple two-state three-modes model of pyrazine shown in Figure 4. The top three pictures show the decay of the S_2 state population for different values of a semiclassical parameter γ in the TDSCF model, the middle panel depicts the mean position of a selected vibrational mode, and the lower panel presents state-specific energies of the two states and the value of the mean coupling. It can be seen that the semiclassical TDSCF method does reasonably well for short times but tends to deteriorate in time, which is typical for mean-field approaches. Part of the discrepancy is also due to problems with zero-point energy conservation in semiclassical TDSCF, which is to a large extent rectified in more recent calculations on similar molecular systems using the mapping formalism.[127,128]

To quantitatively simulate the absorption spectrum, a more accurate MCTDH approach is adopted.[66] The starting point of this calculation of the dynamics of the $S_2 \leftarrow S_0$ photoexcited pyrazine[157,158] has been a system−bath division where only four crucial vibrational modes are accurately included while the remaining vibrational modes of the system are treated in a cruder way as harmonic or Morse oscillators. The coordinates of choice are the normal modes of the electronic ground state, and the coupling between the S_1 and S_2 surfaces is treated in a diabatic representation. It has been shown in this study that the system−bath interaction cannot be accurately described within a mean-field approximation and a multiconfiguration wave function is necessary for proper description of the energy exchange between the system and the bath, for determining the rate of interstate crossing, and, as already mentioned, for modeling the spectrum via a Fourier transform of the autocorrelation function. Figure 5 depicts the $S_2 \leftarrow S_0$ absorption spectrum for different numbers of bath oscillators included in the simulation. The finite widths of the individual peaks directly relate to the lifetime of the internal conversion process. The bath tends to wash out the vibrational structure of the

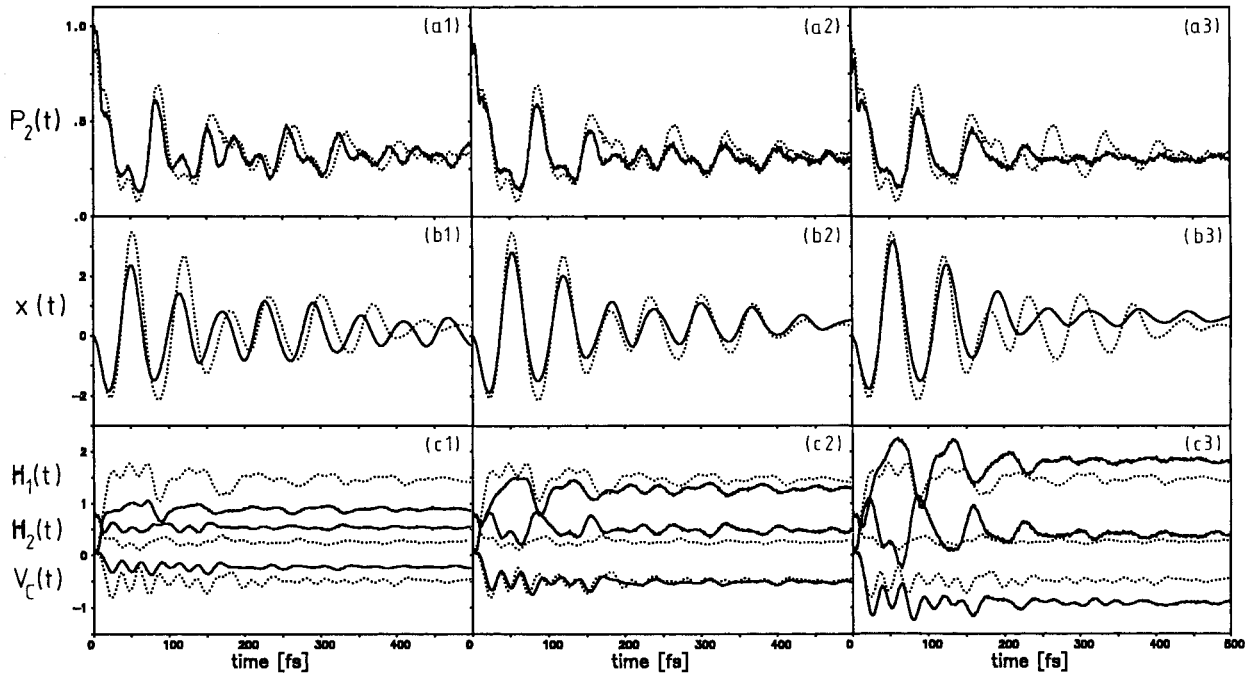

Figure 4. Comparison of the results obtained by semiclassical simulations (—) and exact quantum calculations (...) for the two-state three modes model of pyrazine. (a) Diabatic population probability $P_2(t)$, (b) mean position $x(t)$ of vibrational mode no. 6, and (c) state-specific energies $H_k(t)$ and $V_c(t)$. The semiclassical parameter $\gamma = 0$ (1), 0.25 (2), and 0.5 (3). (Reprinted with permission from ref 156. Copyright 1995 American Institute of Physics.)

spectrum. Most of this is accomplished by the first 10 bath modes, although for a converged description all 20 bath oscillators have to be included. The converged spectrum, though significantly broadened, still shows distinct vibrational resonances.

C. Electron Photodetachment in the I^-Ar_n (n = 2–12) Clusters

A necessary ingredient for quantitative studies of weakly bound complexes is an accurate knowledge of the corresponding potential energy surfaces. High-resolution spectroscopic measurements provide a direct tool for determining the interatomic interactions in such systems. The zero electron kinetic energy (ZEKE) method, which is a type of photoelectron spectroscopy with vibrational resolution, of anionic clusters such as X^-Rg_n (where X^- is a halogen anion and Rg a rare gas atom) provides information about both the anionic and neutral potential energy surfaces.[159,160] As seen in Figure 6, there are actually four surfaces involved, one anionic and three low-lying neutral potentials, resulting from the three possible orientations of the p orbital of the halogen atom. The neutral surfaces are further split by spin–orbit coupling.

The ZEKE spectra of the three smallest I^-Ar_n clusters are depicted in Figure 7. All three neutral states are clearly resolved in the spectra with prominent vibrational structures. The origins of the *X* and *II* states are significantly blue-shifted relative to the corresponding atomic lines, indicating that the anionic clusters are more strongly bound than their neutral counterpart. Enlarging the cluster size results in a further blue-shift of the band origins, broadening of the spectra, and gradual loss of the vibrational structure, primarily due to a more efficient intracluster vibrational redistribution.

The experimental ZEKE spectra were modeled by several quantum dynamical methods via the Fourier transform of the autocorrelation function. Photodetachment in clusters with 2–6 argon atoms[161] has been studied using the cellularized frozen Gaussian approximation.[101] As shown in Figure 8, the resulting spectra for the *X* and *I* surfaces are in a fairly good agreement with the experiment. Part of the remaining discrepancies can be attributed to the presence of hot bands which have not been accounted for in the simulation.

ZEKE spectra for a small I^-Ar_2 cluster and large I^-Ar_{12} complex have also been modeled using the CSP method.[76,162] In accord with the experiment, the suppression of the vibrational structure upon enlarging the system is observed.[76] An interesting problem appears when evaluating the details of the spectrum in the small system. Namely, the quality of the CSP approximation deteriorates in time and the simulation has to be stopped before a sufficiently long autocorrelation function is generated for determining a well-resolved spectrum via the Fourier transform. A remedy for this problem is the use of the filter-diagonalization method,[163–167] which allows one to extract spectra from very short time signals. Figure 9 shows the ZEKE spectrum of the *I* band for the I^-Ar_2 cluster calculated by the CSP method and numerically exactly. It can be seen that the filter-diagonalization method correctly recovers the main $0 \leftarrow 0$ peak as well as the vibrational progression from the short-time CSP signal. The result is in a very good agreement with the experiment except that again the simulations do not account for the presence of hot bands in the measured ZEKE spectra.

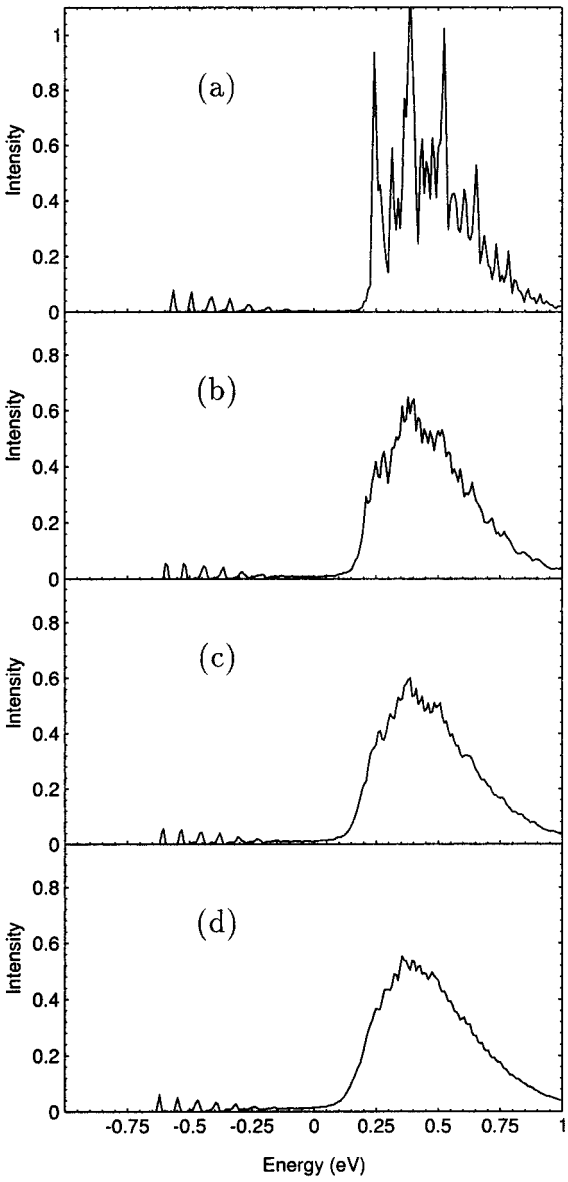

Figure 5. Absorption spectra for a model of the S_1 and S_2 states of the pyrazine molecule after excitation to the S_2 state, coupled to harmonic oscillator baths of varying size: (a) 0 bath oscillators, (b) 5 bath oscillators, (c) 10 bath oscillators, (d) 20 bath oscillators. (Reprinted with permission from ref 158. Copyright 1998 American Institute of Physics.)

D. Relaxation and Raman Spectroscopy of Photoexcited I_2 in Rare Gas Environment

The photoinduced dissociation of the I_2 molecule in various solid, liquid, cluster, or gas environments is considered as a prototype of the cage effect,[168] where the solvent hinders the dissociation process. The I_2 molecule is especially suitable from an experimental point of view since it strongly absorbs in visible regions accessible by common lasers and is also very interesting for having, due to a significant spin−orbit mixing, a plethora of optically accessible low-lying excited states. Out of these electronic states, the most thoroughly studied have been excitations from the ground $X(^1\Sigma_g^+)$ state to a weakly bound $B(^3\Pi_{0u}^+)$ state and to essentially repulsive $B''(^1\Pi_{1u})$,

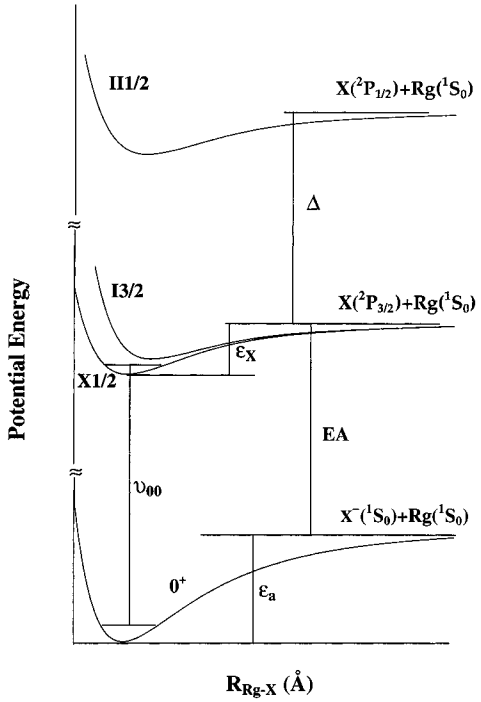

Figure 6. Anionic and the three lowest neutral potential energy curves of the halogen−rare gas complex. (Reprinted with permission from ref 159. Copyright 1994 American Institute of Physics.)

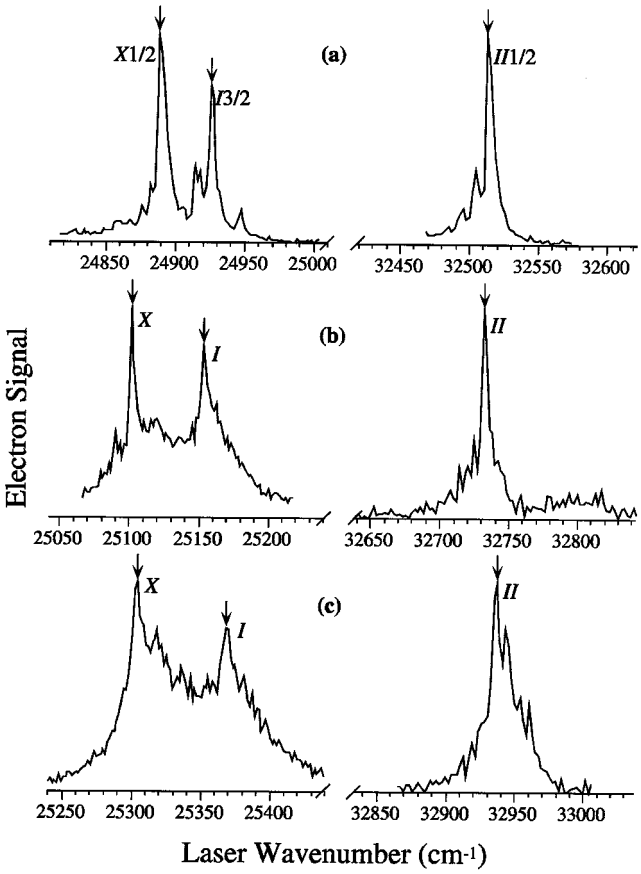

Figure 7. ZEKE spectra of (a) I^-Ar, (b) I^-Ar_2, and (c) $I-Ar_3$. The arrows indicate the neutral electronic state origins. (Reprinted with permission from ref 160. Copyright 1996 American Institute of Physics.)

$a(^3\Pi_g)$, and $a'(^3\Sigma_g^-)$ states. The shapes of these potential curves[169,170] are depicted in Figure 10.

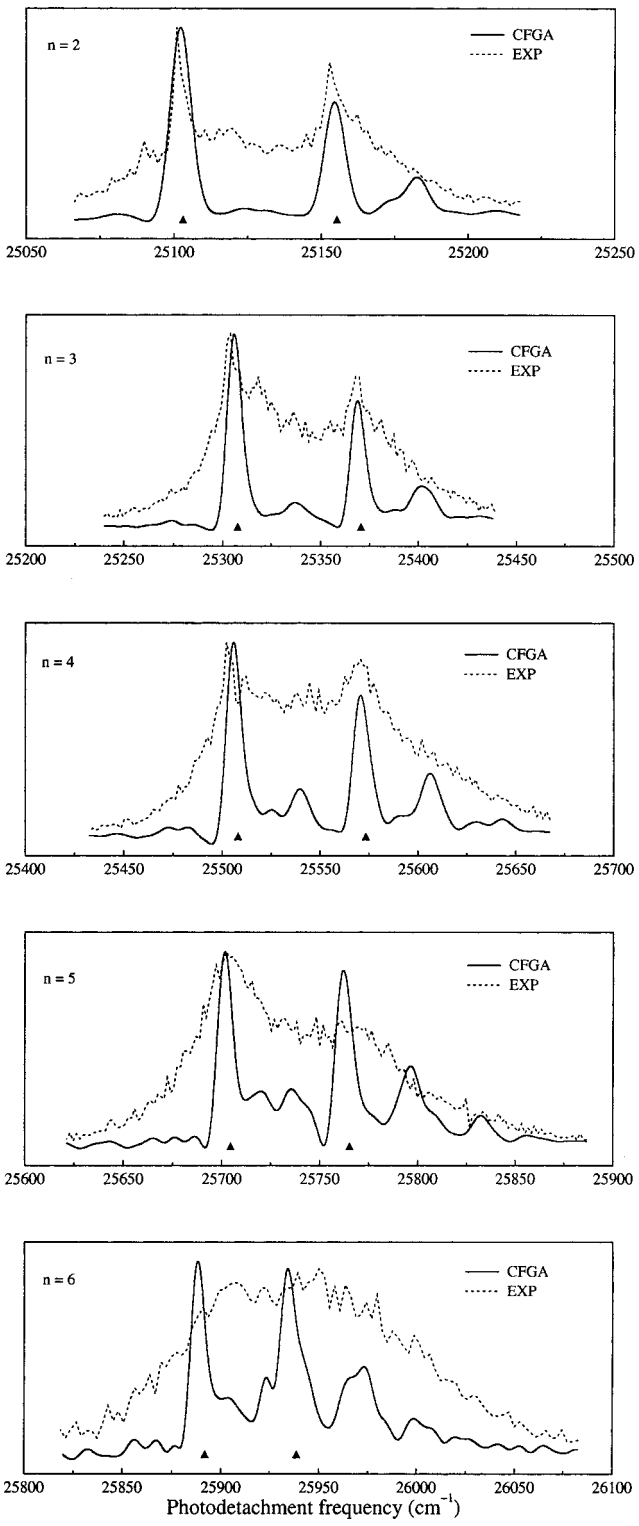

Figure 8. Comparison of the calculated (CFGA) and experimental photodetachment spectra of I^-Ar_n ($n = 2-6$). (Reprinted with permission from ref 161. Copyright 1997 American Institute of Physics.)

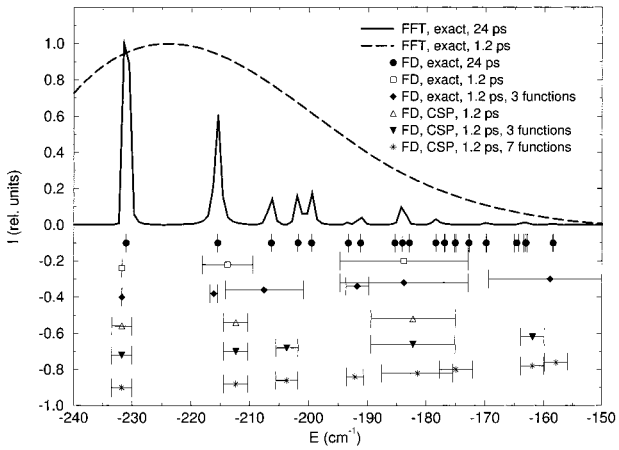

Figure 9. Vibrationally resolved photodetachment spectrum of I^-Ar_2 corresponding to the $I_{3/2}$ neutral state. Comparison between spectra obtained using FFT and filter-diagonalization for long- and short-time numerically exact and CSP propagations. (Reprinted with permission from ref 162. Copyright 1997 Elsevier Science.)

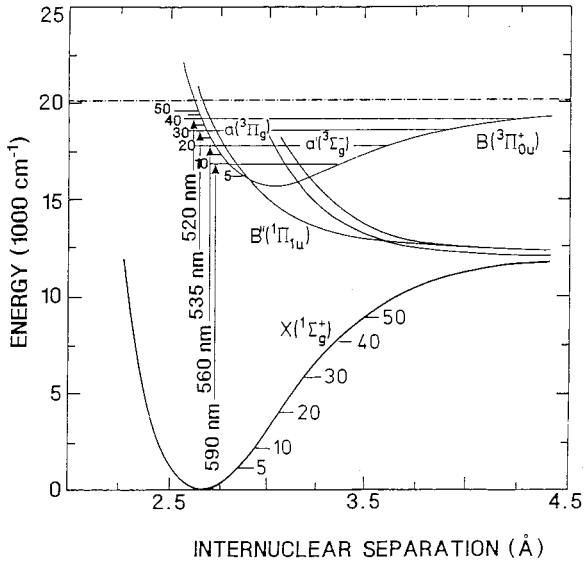

Figure 10. Relevant potential energy surfaces of I_2 showing vibrational levels together with several wavelengths chosen for excitation. (Reprinted with permission from ref 170. Copyright 1994 American Institute of Physics.)

Resonance Raman spectra of the I_2 molecule have been measured in rare gas matrixes[171−173] as well as in liquids such as xenon, CCl_4, and others.[170,174] Typically, the spectra show long and sometimes nonmonotonic overtone progressions. The more recent Raman measurements have been directed toward elucidating the underlying vibronic dynamics on very short time scales. In parallel, pump−probe measurements have been carried out for these systems together with classical and semiclassical MD simulations in order to directly monitor the subpicosecond photodissociation dynamics in a solvent and possibly influence it by shaping the laser pulses.[175−180] In the femtosecond experiments, the low-lying excited states are pumped while probing is done by exciting higher ion-pair states and detecting the fluorescence from these states. In this way, information is gained about the evolution of the population on the pumped state which can be rationalized in terms of electronic and vibrational predissociation. By proper tailoring (chirping) of the optical pulses, the I_2 wave function can be kept localized for a relatively long time, even in the rare gas matrix, and the breaking and remaking of the I−I bond near the dissociation threshold can be controlled.[176] The MD simulations show that trajectory ensembles can go a long way in modeling these condensed phase processes, and some behavior

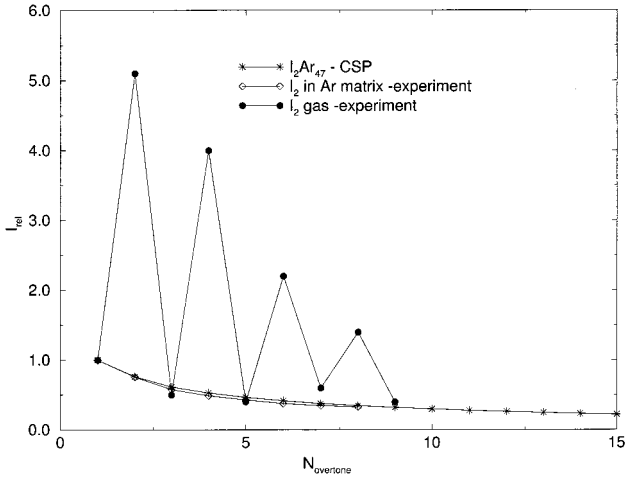

Figure 11. Calculated resonance Raman overtone intensities for the $I_2(B)Ar_{47}$ cluster, compared to matrix and gas-phase experimental data. (Reprinted with permission from ref 21. Copyright 1997 Elsevier Science.)

that could be mistakenly attributed to quantum delocalization and interferences is nothing but a spreading of classical trajectories.

Several approximate quantum dynamical methods have been applied to the study of ultrafast relaxation of the photoexcited I_2 molecule in a solvent. A mixed quantum−classical TDSCF method has been used to study the dynamics of model collinear I_2 Ar_n and I_2-Kr_n chains.[181] The I−I dynamics is treated quantum mechanically, while the rare gas bath atoms are described using classical trajectories. These calculations predict a significant energy transfer from the I_2 species to the solvent and, despite the crudeness of the collinear chain approximation, show that coherence in the recombined I−I wave function is not completely destroyed, in agreement with experiment.

Resonance Raman spectra for the I_2Ar_{17} and I_2Ar_{47} clusters representing the first and second solvation shells around the I_2 solute have been modeled using the CSP method.[21,78] The solvent has a pronounced effect on the resonance Raman spectra. Namely, due to the dephasing of the solvent modes by collisions with the iodine atoms, the oscillatory shape of the gas-phase Stokes progression is practically completely suppressed (see Figure 11). These collisions occur roughly 100 fs after photoexcitation to the B state, and within this period the resonance Raman spectrum is determined. Figure 11 also shows the comparison with the spectrum measured in the argon matrix. The very good agreement indicates first that the two solvation shells have a very similar effect on the spectra as the matrix and second that the separable CSP method is appropriate in this case.

In considerable detail, the resonance Raman spectra have also been studied via the mixed-order semiclassical molecular dynamics.[103,182] As in the CSP simulations described above, the effect of the cage dephasing on the suppression of oscillations in the Raman progression has been observed. A significant improvement of the agreement with the experimental spectrum has been achieved by considering more than one excited surface. Namely, it turns out that signals originating from the B and B″ states cannot

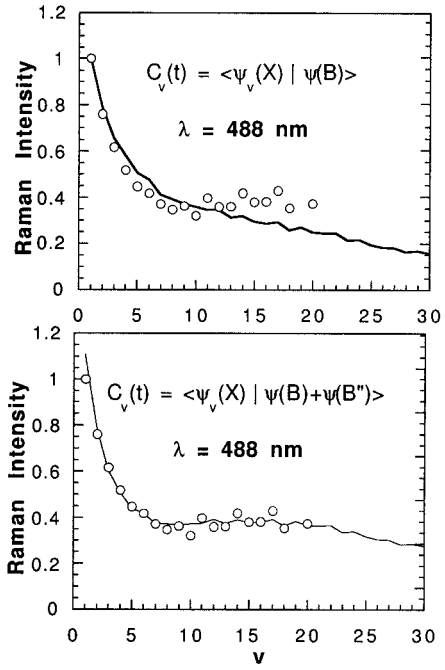

Figure 12. Comparison between experiment and simulation of resonance Raman intensities of I_2 in solid krypton. Top panel: single-surface simulation. Bottom panel: two-surface simulation. (Reprinted with permission from ref 182. Copyright 1997 American Institute of Physics.)

be separated at certain excitation wavelengths. Figure 12 demonstrates how the experimental Raman progression is accurately reproduced when both the B and B″ states are taken into account, while considering the B state only does not lead to a quantitative agreement with the experiment.

Finally, a longer 500 fs dynamics corresponding to several I−I vibrations in the Ar_{17} cage has been studied using the CI−CSP approach.[83] It has been shown that separability of the wave function breaks upon the first collision with the argons and about a thousand configuration interaction terms are necessary to describe the intermode correlations at this timescale. The CI−CSP calculations also show that the energy transfer from the I_2 (B) species to the solvent is very efficient and highly mode-specific. This is demonstrated in Figure 13 which shows the time evolution of the kinetic energy of the I−I mode and the solvent degrees of freedom. It can be seen that the solvent acquires about 0.15 eV during the first solute−solvent collision. Not surprisingly, the modes which pick up most of the kinetic energy are those with large amplitude motions along the I−I coordinate.

E. Rotational Control of HCl Photodissociation in Argon Clusters

The cage effect for photodissociating hydrogen halides in rare gas environment differs significantly from that of the I_2 molecule discussed in the previous subsection. The first excited state of hydrogen halides is much more repulsive; therefore, the light hydrogen atom acquires a large velocity during the photolysis and the trapping by the solvent is significantly less efficient. Nevertheless, evidence for the cage effect

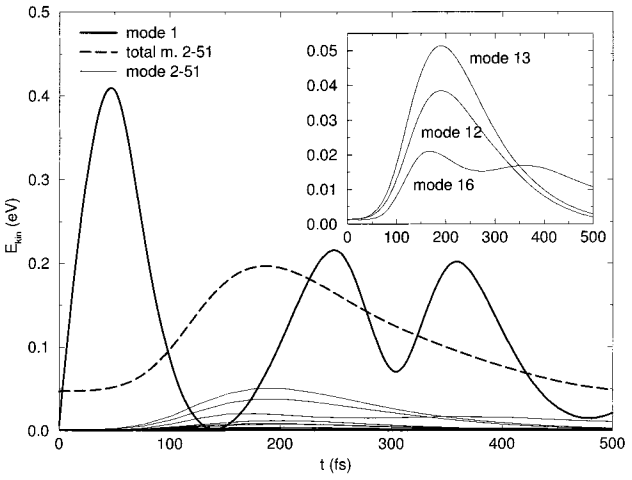

Figure 13. Single-mode CI−CSP kinetic energies during the relaxation of I_2 in Ar_{17}. Insert shows the three most important cage modes on a finer energy scale. (Reprinted with permission from ref 83. Copyright 1997 American Institute of Physics.)

even for a single solvent atom has been given experimentally by measuring the hydrogen kinetic energy distribution resulting from UV photodissociation of the HBr molecule in the Ar−HBr cluster.[183] Compared to the bare HBr molecule, the kinetic energy distribution in the cluster has a tail extending toward lower energies which clearly shows that the photodissociating hydrogen atom is slowed by the rare gas atom.

Another interesting feature concerning hydrogen halide molecules solvated in a cryogenic rare gas environment is the large amplitude motion of the hydrogen atom perpendicular to the hydrogen halide molecular axis. The cold and light hydrogen atom in a shallow intermolecular potential behaves as a strongly delocalized quantum particle. Depending on the size of the system and position of the solute, hydrogen motions ranging from a large amplitude bending (e.g., in the collinear Ar···HCl cluster) to an almost free rotation (e.g., HCl inside the icosahedral Ar_{12} cluster) have been observed.[184,185] Also, there is a large difference in the spatial hydrogen density between the ground and low-lying excited (hindered) rotational states[186,187] which brings up the idea of controlling the cage effect by far-IR rotational preexcitation of the solvated HCl molecule prior to photolysis. The shapes of the three lowest symmetrically allowed rotational states of the HCl molecule embedded in an icosahedral Ar_{12} cluster representing the first solvation shell are depicted in Figure 14. It can be seen that the lowest rotational state is practically isotropic. On the other hand, the first symmetrically allowed excited state has its hydrogen density oriented primarily toward the argons while in the second excited state the hydrogen points mainly to the holes in the cage. Therefore, a stronger cage effect is expected in the former case and a larger extent of direct dissociation in the latter case upon photolysis of the HCl bond.

The ultrafast dynamics of the photoexcited $HClAr_{12}$ cluster has been investigated by methods based on the CSP approximation.[82] For the study of the light particle, a fully coupled 3-dimensional description of the hydrogen atom interacting with a separable cage has been employed. The hydrogen wave function has been described in spherical coordinates, and normal modes have been employed for the cage including the

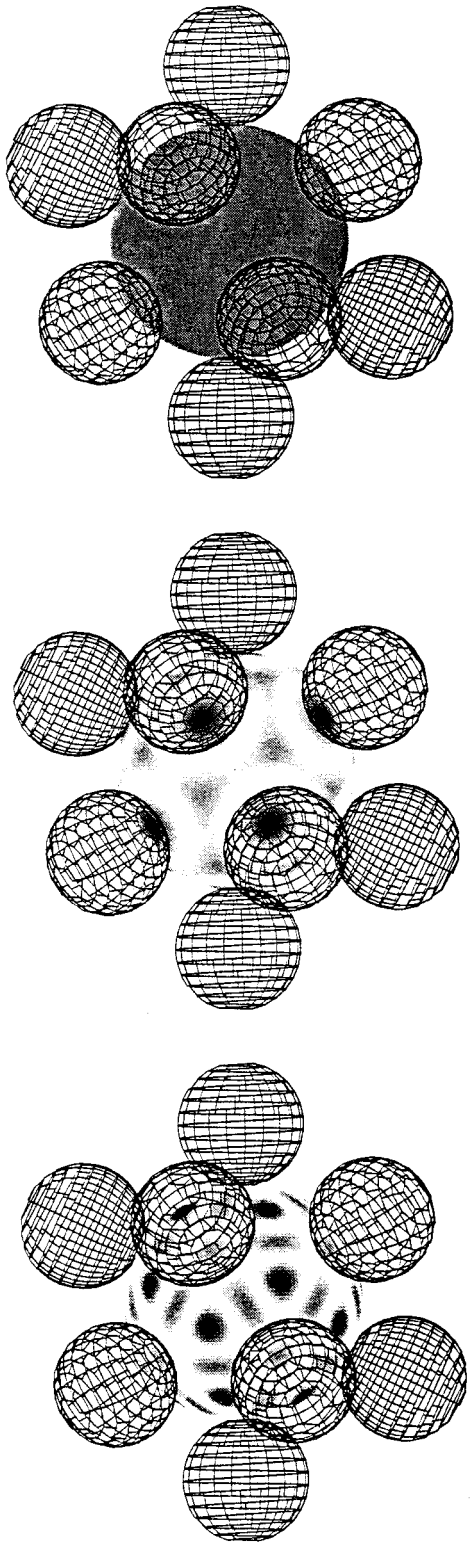

Figure 14. Three lowest totally symmetric rotational wave functions of the HCl molecule embedded in an icosahedral Ar_{12} cluster. The shadowing on the inner spheres corresponds to the probability of a certain orientation of the HCl molecule, while the outer spheres represent the argon atoms. (Reprinted with permission from ref 82. Copyright 1999 American Institute of Physics.)

chlorine atom. For the study of the energy transfer to the cage, the mean-field treatment of the solute−solvent interaction has proven to be insufficient and the nonseparable post-averaging CSP method[77] has been applied. The time evolution of the radial part of the hydrogen wave function for the three different initial rotational states is shown in Figure 15. There is a pronounced difference between the three cases. Starting from the ground rotational state, most of the hydrogen dissociates practically directly with only a minor interaction with the cage. Only a small part gets significantly deflected or even temporarily trapped. Starting from the first excited rotational state, the trapping is much more efficient, while in the case of the second excited initial rotational state, practically all the hydrogen wave function directly dissociates. This has a significant effect on measurable quantities such as the temporary hydrogen populations in the cage or the final kinetic energy distribution of the hydrogen atom. After the first collision with the cage there is about 5 times more hydrogen left in the cage for the first excited rotational state compared to the second one. In the kinetic energy distribution, this is reflected in the former case by a more pronounced structure due to the presence of short-lived vibrational resonances.

F. Absorption Line Shapes of Electrons Solvated in Sodalites

It has been realized for a long time that zeolites, dry sodalites, and halogen sodalites change color when exposed to alkali atom vapor.[188−191] The mechanism in sodalites consists of ionization of the absorbed sodium atom producing Na^+ and an electron, which is shared by the neighboring sodium atoms already present in the cage. The color change is then due to the shared electron which absorbs in the visible range. Evidence for this mechanism has been given by electron spin resonance and electron spin−echo measurements.[188,191] The system can be viewed as consisting of an electronic color center in a host lattice, the specific choice of which influences the position of the peak in the absorption spectrum.

The experimental absorption spectrum has been modeled by a quantum wave function propagation and a subsequent Fourier transform of the autocorrelation function.[192] The nuclear dynamics has been described within the frozen Gaussian wave packet method,[93,193] and the electronic wave function has been treated in an adiabatic approximation.[194] The total autocorrelation function decays to zero in about 20 fs but shows weak recurrences around 140 and 280 fs which can be ascribed to the breathing mode of the sodalite. It is, however, possible that these recurrences are to a large extent artifacts of the separable approximation which tends to underestimate the interactions between the vibrational modes and the consequent dephasing of the wave function. Therefore, two versions of the resulting absorption spectrum are depicted in Figure 16, a high-resolution spectrum using a 350 fs simulation and a low-resolution spectrum which neglects the recurrences by taking into account only the first 50 fs. The peak position and general shape of the low-resolution

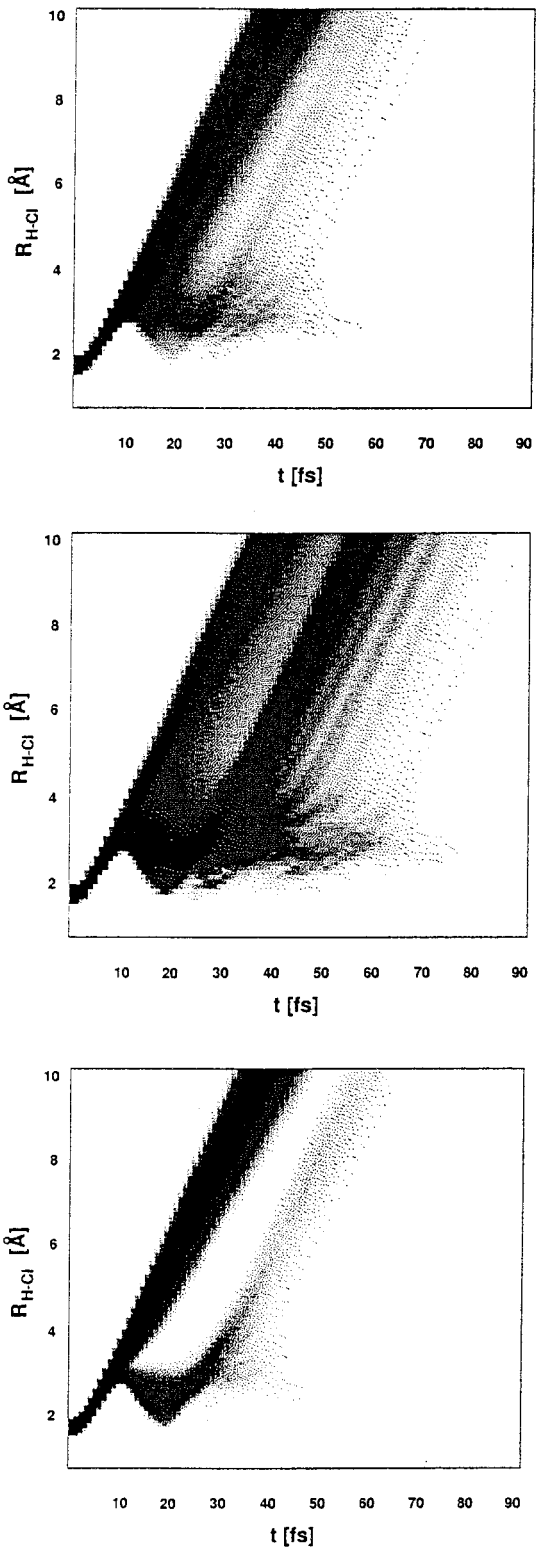

Figure 15. HCl photolysis in the Ar_{12} cluster−quantum dynamics of the radial hydrogen wave function for three different initial rotational states. Note that the wave function bifurcations induced by collisions with the argon cage are very different for the three initial rotational states. (Reprinted with permission from ref 82. Copyright 1999 American Institute of Physics.)

spectrum are in good agreement with the experiment. However, the homogeneous line width of the simulated spectrum which is due to the nuclear motions is about a factor of 2 smaller than the width of the

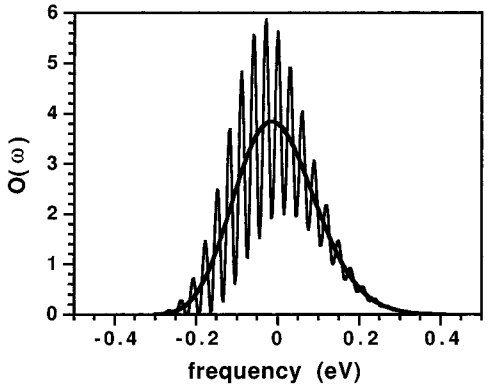

Figure 16. Low- and high-resolution absorption spectra for one of the T_2 states of the color center in chloro-sodalites obtained as a Fourier transform of the nuclear overlap over a sampling period of 50 or 350 fs. (Reprinted with permission from ref 192. Copyright 1995 American Institute of Physics.)

experimental spectrum. This indicates that the measured spectrum is broadened inhomogeneously, possibly by the material disorder in the experimental samples.

G. Hydrogen Diffusion in Crystalline Silicon

Lattice impurities can strongly influence the behavior of semiconductor materials. In particular, the mobility of reactive hydrogen or deuterium changes optical and electrical properties of silicon crystals. A considerable effort has, therefore, been directed toward studying the dynamical aspects, namely, the diffusivity of hydrogen impurities in crystalline silicon. High-temperature experiments show an Arrhenius dependence of the diffusion coefficient, which indicates the presence of an activation barrier of roughly 0.5 eV.[195] On the other hand, at lower temperatures reaction rates smaller by several orders of magnitude than those following from the Arrhenius curve have been observed.[196−198] This anomaly has been traditionally attributed to a switch of the diffusion mechanism to non-nearest-neighbor hops above a certain critical temperature.[197]

The problem of hydrogen and deuterium diffusion in silicon has been recently addressed by the quasi-adiabatic propagator path−integral method with a special emphasis on elucidating the importance of quantum dynamical effects in the process under study.[199] Except for extremely low temperatures, hydrogen diffusion is an incoherent process which involves jumps between stable sites. This process can therefore be described by a rate equation. The diffusivity coefficient is directly related to the corresponding rate constant k evaluated as a time integral of a flux−flux correlation function.[200−202] It is this correlation function which is evaluated using the dynamic path−integral method with a system(hydrogen)−bath(silicon crystal) Hamiltonian.[137]

The results of the present calculations have been compared to classical simulations as well as to previous experimental and theoretical findings. Figure 17 depicts the hydrogen diffusion rate obtained by different methods as a function of inverse temperature. The main findings and conclusions are as

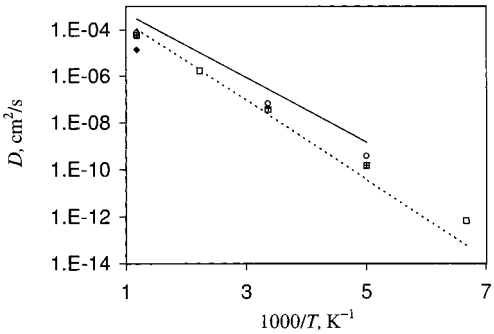

Figure 17. Hydrogen diffusion rate in crystalline silicon as a function of inverse temperature: (—) transition-state theory estimate, (- - -) transition-state theory estimate for the one-dimensional adiabatic model, (+) path integral results, (□) path integral results for the one-dimensional adiabatic model, (○) classical trajectory results employing the two-dimensional reaction surface, (◊) experiment. (Reprinted with permission from ref 199 after minor corrections suggested by the authors of ref 199. Copyright 1998 American Institute of Physics.)

follows: Lattice vibrations strongly couple to the hydrogen motion, which results in a decrease of the diffusion rate compared to the prediction of the transition-state theory. Quantum mechanical phenomena, especially tunneling and zero-point motions, have a significant contribution to the diffusion rate even at room temperature. Finally, an increase of the quantum mechanical diffusion rate of deuterium relative to hydrogen, i.e., a negative isotope effect, is observed at intermediate temperatures in agreement with experimental findings on boron-doped silicon.[203] This effect is attributed to an increase of the zero-point energy in the vicinity of the transition state.

H. Retinal Photoisomerization in Bacteriorhodopsin

Probably the largest system addressed so far by approximate quantum dynamical methods is bacteriorhodopsin, which is a protein involved in photosynthetic energy storage, light absorption, and energy conversion.[204−206] This protein is also closely related to rhodopsin, which is the light detector in visual processes. The structure of bacteriorhodopsin is schematically shown in Figure 18.

Bacteriorhodopsin represents a benchmark system for studying protein function and dynamics. Its structure, which has been determined with great accuracy and detail, shows a pathway for transport of protons released by photoexcitation through the protein.[207−209] The principal question addressed by the quantum simulations concerns the proton pump mechanism. In other words, the problem can be stated as follows: How is the proton-transfer coupled to light absorption? Without going into detail, the proton pathway is connected with all-*trans* to 13-*cis* isomerization of the retina. This isomerization is an ultrafast elementary physical process which takes place on three coupled electronic surfaces.

The computational scheme adopted for treating the above ultrafast nonadiabatic process is the multiple spawning method.[120−126] A traveling Gaussian basis is set on each of the coupled surfaces, and the total wave function is written as a linear combination of

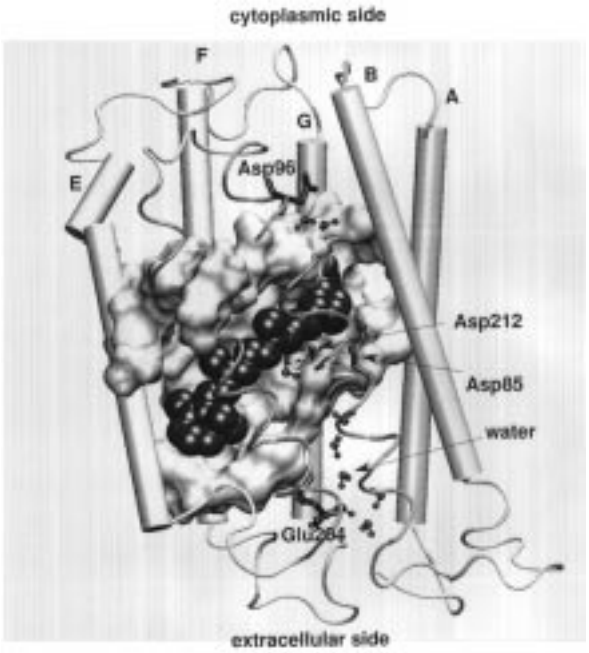

Figure 18. Schematic picture of bacteriorhodopsin and retinal binding site. Retinal is shown in a van der Waals sphere representation, and part of the nearby residues are shown in a surface representation. Transmembrane helices A, B, E, F, G are shown as cylinders and helices C and D are shown as thin tubes to reveal the retinal binding site. Note that the rendering of the retinal, for the sake of clarity, does not show hydrogen atoms; as a result retinal appears less voluminous than in reality. (Reprinted with permission from ref 205. Copyright 1998 The Royal Society of Chemistry.)

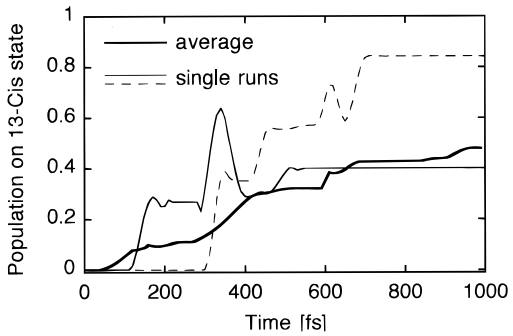

Figure 19. Population on the 13-*cis* electronic state as a function of time: (—) average result; (— and - - -) two typical single runs. Note that whereas the average population transfer increases monotonically, significant back-transfer is observed in single runs. (Reprinted with permission from ref 205. Copyright 1998 The Royal Society of Chemistry.)

these basis functions. The principal result is the time evolution of the population of the product 13-*cis* electronic state shown in Figure 19. The spawning method predicts a smooth population transfer, most of which is taking place during the first 300 fs with some transfer taking up to 1 ps. The final population of this state is approximately 48%, which is in a reasonable accord with the experimental value of 64 ± 4%.[210] An important result of the simulations is the observation that photoisomerization takes place in two opposite rotational senses which lead to different photoproducts, only one of which is likely to trigger the proton pumping.

Finally, we note that the accuracy of the reported simulations remains to be determined. A rather limited Gaussian expansion for a system with more than 10^4 degrees of freedom is likely not to be fully converged. Consider, for example, the initial wave function which is represented by a sum of 16 terms, each of which being a product Gaussian in Cartesian coordinates. A representative wave function for the system under study at ambient temperatures is estimated to have, due to thermally excited soft modes, many hundreds of peaks, certainly much more than can be described by the limited basis set.

The above argument shows how different general considerations for large and small systems can be and how essential it is to develop error estimates for methods tailored to large systems. It is, of course, quite possible that methods will work well despite limited basis sets or other approximations, but this can be settled only when errors are studied and at least estimated—a major challenge and limitation for this entire field.

VI. Summary and Conclusions

The present paper has reviewed quantum dynamical simulation methods which are practical for investigations of fast processes in large polyatomic systems. Special emphasis has been paid to applications where theory has significantly contributed to the interpretation of both time-domain and frequency-domain experiments. One of the goals of the authors has been to convince the reader that quantum effects are important in the dynamics of large atomic and molecular systems and that there is a great need for computational methods capable of accounting for the quantum nature of the dynamical processes at a quantitative level.

It has been shown that practical quantum methods treating polyatomic systems are inevitably of an approximate character. Introduction, to a certain extent, of classical concepts simplifies the calculations enormously and is well-justified for most problems in chemical physics where quantum effects tend to be moderate. Other simplifications go along the line of the mean-field approximation, which works well for ultrafast processes and for systems with good separation of mode frequencies. Most likely future methods will also dwell on these powerful approximations. For systems with moderate quantum effects, classical mechanics as an auxiliary tool can tell us where the most important correlations are and including only these in a subsequent quantum simulation can help to overcome the exponential scaling of the numerical effort with system size. Building correlated wave functions from separable fragments has an additional advantage of a very intuitive interpretation in terms of single-mode dynamical properties. Another promising approach is to directly construct a nonseparable quantum dynamical model, skipping the mean-field separable step. This leads to different variants of the real time path integral method where classical trajectories are potentially very useful in numerically stabilizing the propagation. One way or another, it is necessary to fight the exponential scaling of numerically exact quantum

dynamics with system size. This is, of course, only possible when the physics itself scales more reasonably, like in the case of ultrafast dynamics of localized wave functions of polyatomic systems.

If the reader has come to the conclusion that the field of quantum molecular dynamics of polyatomic systems is an exciting area of research, certainly far from maturity but full of potential, then the review has fulfilled its purpose.

VII. Acknowledgment

We would like to thank above all our present and former students and postdocs Petra Zdánská, Martina Roeselová, Joon Jung, Erick Fredj, Rami Rom, and Jeremy Harvey. We also thank Burkhard Schmidt, Udo Buck, Nancy Makri, Hans-Dieter Meyer, Gerhard Stock, and Ara Apkarian for fruitful discussions. Support by Grant no. A4040706 from the granting agency of the Academy of Sciences of the Czech Republic, by an NSF International/Czech government grant (Grant no. 445944-21210/ES010), by the Chemistry Division of the NSF, the Israel Science Foundation, the Israel Ministry of Science, and by the SFB no. 450 from the DFG Germany is gratefully acknowledged.

VIII. References

(1) Schinke, R. *Photodissociation Dynamics*; Cambridge University Press: Cambridge, 1993.
(2) Zhang, D. H.; Zhang, J. Z. K. *J. Chem. Phys.* **1994**, *100*, 2679.
(3) Kouri, D. J.; Houng, Y.; Zhu, W.; Hoffman, D. K. *J. Chem. Phys.* **1994**, *100*, 3362.
(4) Peskin, U.; Moiseyev, N. *J. Chem. Phys.* **1993**, *99*, 4590.
(5) Neuhauser, D. *J. Chem. Phys.* **1994**, *100*, 9272.
(6) Manthe, U.; Seideman, T.; Miller, W. H. *J. Chem. Phys.* **1990**, *92*, 10078.
(7) Zang, J. Z. H.; Miller, W. H. *J. Chem. Phys.* **1990**, *92*, 811.
(8) Kosloff, R. *Annu. Rev. Phys. Chem.* **1994**, *45*, 145.
(9) Schatz, G. C. *J. Phys. Chem.* **1996**, *100*, 12839.
(10) *Femtosecond Chemistry*; Manz, J., Woste, L., Eds.; Wiley-VCH: Weinheim, 1994.
(11) *Femtochemistry*; Chergui, M., Ed.; World Scientific: Singapore, 1996.
(12) *Femtochemistry and Femtobiology*; Sundstrom, V., Ed.; World Scientific: Singapore, 1998.
(13) Gerber, R. B.; Kosloff, R.; Berman, M. *Comput. Phys. Rep.* **1986**, *5*, 59.
(14) Leforestier, C.; Bisseling, R. H.; Cerjan, C.; Feit, M. D.; Friesner, R.; Guldberg, A.; Hammerich, A.; Jolicard, G.; Karrlein, W.; Meyer, H.-D.; Lipkin, N.; Roncero, O.; Kosloff, R. *J. Comput. Phys.* **1991**, *94*, 59.
(15) Kulander, K. C. *Comput. Phys. Commun.* **1991**, *63*, 1−584.
(16) Kosloff, R. In *Dynamics of Molecular and Chemical Reactions*; Wyatt, R. E., Zhang, J. Z. H., Eds.; Marcel Dekker: New York, 1996; p 185.
(17) Allen, M. P.; Tildesley, D. J. *Computer Simulations of Liquids*; Clarendon Press: Oxford, 1987.
(18) Whitnell, R. M.; Wilson K. R. *Rev. Comput. Chem.* **1993**, *4*, 67.
(19) Warshel, A. *Computer modeling of chemical reactions in enzymes and solutions*; Wiley: New York, 1991.
(20) Brooks, C. L., III; Karplus, M.; Pettitt, B. M. *Adv. Chem. Phys.* **1988**, *71*, 1.
(21) Jungwirth, P.; Fredj, E.; Zdanska, P.; Gerber, R. B. *Comput. Chem.* **1997**, *21*, 419.
(22) Schatz, G. C.; Ratner, M. A. *Quantum Mechanics in Chemistry*; Prentice Hall: New York, 1993.
(23) Light, J. C.; Hamilton, I. P.; Lill, J. V. *J. Chem. Phys.* **1985**, *82*, 1400.
(24) Sharafeddin, O. A.; Light, J. C. *J. Chem. Phys.* **1995**, *102*, 3622.
(25) Sim, E.; Makri, N. *J. Chem. Phys.* **1995**, *102*, 5616.
(26) Kosloff, D.; Kosloff, R. *J. Comput. Phys.* **1983**, *52*, 35.
(27) Kosloff, R.; Kosloff, D. *J. Chem. Phys.* **1983**, *79*, 1823.
(28) Temperton, A. *J. Comput. Phys.* **1983**, *52*, 1.
(29) Tal-Ezer, H.; Kosloff, R. *J. Chem. Phys.* **1984**, *81*, 3967.
(30) Peskin, U.; Kosloff, R.; Moiseyev, N. *J. Chem. Phys.* **1994**, *100*, 8849.
(31) Yao, G.; Wyatt, R. E. *J. Chem. Phys.* **1994**, *101*, 1904.
(32) Huang, Y.; Chu, S. I. *Chem. Phys. Lett.* **1994**, *225*, 46.
(33) Howland, J. S. *Math. Ann.* **1974**, *207*, 315.
(34) Pfeifer, P.; Levine, R. D. *J. Chem. Phys.* **1983**, *79*, 5512.
(35) Yao, G.; Wyatt, R. E. *Chem. Phys. Lett.* **1995**, *239*, 207.
(36) Guiang, C. S.; Wyatt, R. E. *Int. J. Quantum Chem.* **1998**, *67*, 273.
(37) Askar, A.; Cakmak, S. *J. Chem. Phys.* **1978**, *68*, 2794.
(38) Yinnon, A. T.; Kosloff, R. *Chem. Phys. Lett.* **1983**, *102*, 216.
(39) Feit, M. D.; Fleck, J. A.; Steiger, A. *J. Comput. Phys.* **1982**, *47*, 412.
(40) Feit, M. D.; Fleck, J. A. *J. Chem. Phys.* **1982**, *78*, 301.
(41) Dirac, P. A. M. *Proc. Cambridge Philos. Soc.* **1930**, *26*, 376.
(42) Heller, E. J. *J. Chem. Phys.* **1976**, *64*, 63.
(43) Harris, R. *J. Chem. Phys.* **1980**, *72*, 1776.
(44) Gerber, R. B.; Buch, V.; Ratner, M. A. *J. Chem. Phys.* **1982**, *77*, 3022.
(45) Makri, N.; Miller, W. H. *J. Chem. Phys.* **1987**, *87*, 5781.
(46) Gerber, R. B.; Ratner, M. A. *Adv. Chem. Phys.* **1988**, *70*, 97.
(47) Messina, M.; Coalson, R. D. *J. Phys. Chem.* **1989**, *90*, 4015.
(48) Haug, K.; Metiu, H. *J. Phys. Chem.* **1993**, *99*, 6253.
(49) Gerber, R. B.; Jungwirth, P.; Fredj, E.; Rom, A. Y. In *Modern Methods for Multidimensional Dynamics Computations in Chemistry*; Thompson, D. L., Ed.; World Scientific: Singapore, 1998.
(50) Peskin, U.; Steinberg, M. *J. Chem. Phys.* **1998**, *109*, 704.
(51) Kucar, J.; Meyer, H.-D.; Cederbaum, L. S. *Chem. Phys. Lett.* **1987**, *140*, 525.
(52) Thompson, T. C.; Miller, W. H. *J. Chem. Phys.* **1982**, *77*, 3031.
(53) Moiseyev, N. *Chem. Phys. Lett.* **1983**, *98*, 233.
(54) Lefebre, R. *Int. J. Quantum Chem.* **1983**, *23*, 543.
(55) Bacic, Z.; Gerber, R. B.; Ratner, M. A. *J. Phys. Chem.* **1986**, *90*, 3606.
(56) Jungwirth, P.; Roeselova, M.; Gerber, R. B. *J. Chem. Phys.* **1999**, *110*, in press.
(57) Miller, W. H.; Handy, N. C.; Adams, J. E. *J. Chem. Phys.* **1980**, *72*, 99.
(58) Fang, J.-Y.; Hammes-Schiffer, S. *J. Chem. Phys.* **1998**, *108*, 7085.
(59) Fang, J.-Y.; Hammes-Schiffer, S. *J. Chem. Phys.* **1998**, *109*, 7051.
(60) Makri, N.; Miller, W. H. *J. Chem. Phys.* **1987**, *87*, 5781.
(61) Blake, N. P.; Metiu, H. *J. Chem. Phys.* **1994**, *101*, 223.
(62) Garcia-Vela, A. *J. Chem. Phys.* **1996**, *104*, 1047.
(63) Meyer, H.-D.; Manthe, U.; Cederbaum, L. S. *Chem. Phys. Lett.* **1990**, *165*, 73.
(64) Hammerich, A. D.; Kosloff, R.; Ratner, M. A. *Chem. Phys. Lett.* **1990**, *171*, 97.
(65) Kotler, Z.; Neria, E.; Nitzan, A. *Comput. Phys. Commun.* **1991**, *63*, 243.
(66) Manthe, U.; Meyer, H.-D.; Cederbaum, L. S. *J. Chem. Phys.* **1992**, *97*, 3199.
(67) Manthe, U. *J. Chem. Phys.* **1994**, *101*, 2652.
(68) Fang, J.-Y.; Guo, H. *J. Mol. Structure—THEOCHEM* **1995**, *341*, 201.
(69) Manthe, U. *J. Chem. Phys.* **1996**, *105*, 6989.
(70) Beck, M. H.; Meyer, H.-D. *Zeit. Phys. D* **1997**, *42*, 113.
(71) Campoz-Martinez, J.; Coalson, R. D. *J. Chem. Phys.* **1990**, *93*, 4740.
(72) Campoz-Martinez, J.; Coalson, R. D. *J. Chem. Phys.* **1993**, *99*, 9629.
(73) Gerber, R. B.; Alimi, R. *Isr. J. Chem.* **1991**, *31*, 383.
(74) Li, Z.; Gerber, R. B. *J. Chem. Phys.* **1993**, *99*, 8637.
(75) Jungwirth, P.; Gerber, R. B. *J. Chem. Phys.* **1995**, *102*, 6046.
(76) Jungwirth, P.; Gerber, R. B. *J. Chem. Phys.* **1995**, *102*, 8855.
(77) Jungwirth, P.; Gerber, R. B. *J. Chem. Phys.* **1996**, *104*, 5803.
(78) Jungwirth, P.; Fredj, E.; Gerber, R. B. *J. Chem. Phys.* **1996**, *104*, 9332.
(79) Jungwirth, P.; Schmidt, B. *Chem. Phys. Lett.* **1997**, *275*, 127.
(80) Wigner, E. *Phys. Rev.* **1932**, *40*, 749.
(81) Hillery, M.; O'Connel, R. F.; Scully, M. O.; Wigner, E *Phys. Rep.* **1984**, *106*, 121.
(82) Zdanska, P.; Schmidt, B.; Jungwirth, P. *J. Chem. Phys.* **1999**, *110*, 6246.
(83) Jungwirth, P.; Fredj, E.; Gerber, R. B. *J. Chem. Phys.* **1997**, *107*, 8963.
(84) Sepulveda, M. A.; Grossmann, F. *Adv. Chem. Phys.* **1996**, *96*, 191.
(85) Herman, M. F. *Annu. Rev. Phys. Chem.* **1994**, *45*, 83.
(86) Kay, K. G. *J. Chem. Phys.* **1994**, *100*, 4377.
(87) Miller, W. H. *J. Chem. Phys.* **1970**, *53*, 3578.
(88) Van Vleck, J. H. *Proc. Natl. Acad. Sci.* **1928**, *14*, 178.
(89) Gutzwiller, M. C. *Chaos in Classical and Quantum Mechanics*; Springer: New York, 1990.
(90) Heller, E. J. *J. Chem. Phys.* **1991**, *94*, 2723.
(91) Herman, M. F.; Kluk, E. *Chem. Phys.* **1984**, *91*, 27.
(92) Herman, M. F. *J. Chem. Phys.* **1986**, *85*, 2069.
(93) Heller, E. J. *J. Chem. Phys.* **1975**, *62*, 1544.
(94) Heller, E. J. *J. Chem. Phys.* **1976**, *65*, 4979.
(95) Huber, D.; Ling, S.; Imre, D. G.; Heller, E. J. *J. Chem. Phys.* **1989**, *90*, 7317.
(96) Herman, M. F. *Chem. Phys. Lett.* **1997**, *275*, 445.

(97) Pechukas, P. *Phys. Rev.* **1969**, *181*, 174.
(98) Feynman, R. P.; Hibbs, A. R. *Quantum Mechanics and Path Integrals*; McGraw-Hill: New York, 1965.
(99) Miller, W. H. *Adv. Chem. Phys.* **1974**, *25*, 69.
(100) Gottfried, K. *Quantum Mechanics*; Benjamin: New York, 1966.
(101) Walton, A. R.; Manolopoulos, D. E. *Mol. Phys.* **1996**, *84*, 961.
(102) Brewer, M. L.; Hulme, J. S.; Manolopoulos, D. E. *J. Chem. Phys.* **1997**, *106*, 4832.
(103) Ovchinnikov, M.; Apkarian, V. A. *J. Chem. Phys.* **1996**, *105*, 10312.
(104) Ovchinnikov, M.; Apkarian, V. A. *J. Chem. Phys.* **1998**, *108*, 2277.
(105) Sun, X.; Miller, W. H. *J. Chem. Phys.* **1996**, *106*, 916.
(106) Tully, J. C.; Preston, P. K. *J. Chem. Phys.* **1971**, *55*, 562.
(107) Herman, M. F. *J. Chem. Phys.* **1982**, *65*, 2949.
(108) Herman, M. F. *J. Chem. Phys.* **1995**, *103*, 8081.
(109) Tully, J. C. *J. Chem. Phys.* **1990**, *93*, 1061.
(110) Webster, F. J.; Rossky, P. J.; Friesner, R. A. *Comput. Phys. Commun.* **1991**, *63*, 494.
(111) Chapman, S. *Adv. Chem. Phys.* **1992**, *82*, 423.
(112) Coker, D. F.; Xiao, L. *J. Chem. Phys.* **1995**, *102*, 496.
(113) Meyer, H.-D.; Miller, W. H. *J. Chem. Phys.* **1979**, *70*, 3214.
(114) Billing, G. D. *Chem. Phys. Lett.* **1975**, *30*, 391.
(115) Micha, D. A. *J. Chem. Phys.* **1983**, *78*, 7138.
(116) Herman, M. F. *Int. J. Quantum Chem.* **1998**, *70*, 897.
(117) Sholl, D. S.; Tully, J. C. *J. Chem. Phys.* **1998**, *109*, 7702.
(118) Hammes-Schiffer, S. *J. Phys. Chem.* **1998**, *102*, 10443.
(119) Billing, G. D. *J. Chem. Phys.* **1997**, *107*, 4286.
(120) Martinez, T.; Ben-Nun, M.; Levine, R. D. *J. Phys. Chem.* **1996**, *100*, 7884.
(121) Martinez, T.; Levine, R. D. *J. Chem. Soc., Faraday Trans.* **1997**, *93*, 940.
(122) Martinez, T.; Ben-Nun, M.; Levine, R. D. *J. Phys. Chem.* **1997**, *101*, 6389.
(123) Martinez, T.; Ben-Nun, M.; Ashkenazi, G. *J. Chem. Phys.* **1996**, *104*, 2847.
(124) Ben-Nun, M.; Martinez, T.; Levine, R. D. *Chem. Phys. Lett.* **1997**, *270*, 319.
(125) Ben-Nun, M.; Martinez, T.; Levine, R. D. *J. Phys. Chem.* **1997**, *101*, 7522.
(126) Ben-Nun, M.; Martinez, T. *J. Chem. Phys.* **1998**, *108*, 7244.
(127) Stock, G.; Thoss, M. *Phys. Rev. Lett.* **1997**, *78*, 578.
(128) Muller, U.; Stock, G. *J. Chem. Phys.* **1998**, *108*, 7516.
(129) Meyer, H.-D.; Miller, W. H. *J. Chem. Phys.* **1979**, *71*, 2156.
(130) Wang, H. B.; Sun, X.; Miller, W. H. *J. Chem. Phys.* **1998**, *108*, 9726.
(131) Sun, X.; Wang, H. B.; Miller, W. H. *J. Chem. Phys.* **1998**, *109*, 7064.
(132) Gallicio, E.; Berne, B. J. *J. Chem. Phys.* **1994**, *101*, 9909.
(133) Kim, D.; Doll, J. D.; Freeman, D. L. *J. Chem. Phys.* **1998**, *108*, 3871.
(134) DePristo, A. E.; Haug, K.; Metiu, H. *Chem. Phys. Lett.* **1988**, *155*, 376.
(135) Luck, A.; Winterstetter, M.; Weiss, U.; Mak. C. H. *Phys. Rev. E* **1998**, *58*, 5565.
(136) Stockburger, J. T.; Mak. C. H. *Phys. Rev. Lett.* **1998**, *80*, 2657.
(137) Makri, N. *Chem. Phys. Lett.* **1992**, *193*, 435.
(138) Makri, N. In *Time-Dependent Quantum Molecular Dynamics*; Broeckhove, J., Lathouwers, L., Eds.; Plenum: New York, 1992; p 209.
(139) Makri, N. *J. Math. Phys.* **1995**, *36*, 2430.
(140) Sim, E.; Makri, N. *J. Phys. Chem. B* **1997**, *101*, 5446.
(141) Cao, J.; Voth, G. A. *J. Chem. Phys.* **1993**, *99*, 10070.
(142) Cao, J.; Voth, G. A. *J. Chem. Phys.* **1994**, *100*, 5106.
(143) Cao, J.; Voth, G. A. *J. Chem. Phys.* **1994**, *101*, 6157.
(144) Cao, J.; Voth, G. A. *J. Chem. Phys.* **1994**, *101*, 6168.
(145) Calhoun, A.; Pavese, M.; Voth, G. A. *Chem. Phys. Lett.* **1996**, *262*, 415.
(146) Buck, U.; Krohne, R.; Lohbrandt, P. *J. Chem. Phys.* **1997**, *106*, 3205.
(147) Buck, U.; Krohne, R. *Phys. Rev. Lett.* **1994**, *73*, 947.
(148) Buck, U.; Meyer, H. *Surf. Sci.* **1985**, *156*, 275.
(149) Brudermann, J.; Lohbrandt, P.; Buck, U.; Buch, V. *Phys. Rev. Lett.* **1998**, *80*, 2821.
(150) Rom, A. Y.; Gerber, R. B. *J. Chem. Phys.* **1997**, *106*, 10168.
(151) Schroder, T.; Schinke, R.; Krohne, R.; Buck, U. *J. Chem. Phys.* **1997**, *106*, 9067.
(152) Fredj, E.; Gerber, R. B.; Ratner, M. A. *J. Chem. Phys.* **1998**, *109*, 4833.
(153) Brudermann, J.; Buck, U.; Fredj, E.; Gerber, R. B.; Ratner, M. A. *J. Chem. Phys.*, submitted for publication.
(154) Innes, K. K.; Ross, I. G.; Moonaw, W. R. *J. Mol. Spectrosc.* **1988**, *132*, 492.
(155) Heller, E. *J. Chem. Phys.* **1978**, *68*, 2066.
(156) Stock, G. *J. Chem. Phys.* **1995**, *103*, 2888.
(157) Worth, G. A.; Meyer, H.-D.; Cederbaum, L. S. *J. Chem. Phys.* **1996**, *105*, 4412.
(158) Worth, G. A.; Meyer, H.-D.; Cederbaum, L. S. *J. Chem. Phys.* **1998**, *109*, 3518.
(159) Zhao, Y.; Yourshaw, I.; Reiser, G.; Arnold, C. C.; Neumark, D. M. *J. Chem. Phys.* **1994**, *101*, 6538.
(160) Yourshaw, I.; Zhao, Y.; Neumark, D. M. *J. Chem. Phys.* **1996**, *105*, 351.
(161) Brewer, M. L.; Hulme, J. S.; Manolopoulos, D. E. *J. Chem. Phys.* **1997**, *106*, 4832.
(162) Jungwirth, P.; Schmidt, B.; Moiseyev, N. *Chem. Phys. Lett.* **1997**, *280*, 177.
(163) Neuhauser, D. *J. Chem. Phys.* **1990**, *93*, 2611.
(164) Pang, J. W.; Neuhauser, D. *Chem. Phys. Lett.* **1996**, *252*, 173.
(165) Mandelshtam, V. A.; Taylor, H. S. *Phys. Rev. Lett.* **1997**, *78*, 3274.
(166) Narevicius, E.; Neuhauser, D.; Korsch, H. J.; Moiseyev, N. *Chem. Phys. Lett.* **1997**, *278*, 250.
(167) Chen, R. Q.; Guo, H. *Phys. Rev. E* **1998**, *57*, 7288.
(168) Franck, J.; Rabinowitsch, E. *Trans. Faraday Soc.* **1934**, *30*, 120.
(169) Mulliken, R. S. *J. Chem. Phys.* **1971**, *55*, 288.
(170) Xu, J.; Schwentner, N.; Chergui, M. *J. Chem. Phys.* **1994**, *101*, 7381.
(171) Howard, W. F.; Andrews, L. *J. Raman Spectrosc.* **1974**, *2*, 447.
(172) Grzybowski, J. M.; Andrews, L. *J. Raman Spectrosc.* **1975**, *4*, 99.
(173) Apkarian, V. A. In *Femtochemistry*; Chergui, M., Ed.; World Scientific: Singapore, 1996.
(174) Sension, R. J.; Strauss, H. L. *J. Chem. Phys.* **1986**, *85*, 3791.
(175) Sterling, M.; Zadoyan, R.; Apkarian, V. A. *J. Chem. Phys.* **1996**, *104*, 6497.
(176) Bardeen, C. J.; Che, J.; Wilson, K. R.; Yakovlev, V. V.; Apkarian, V. A.; Martens, C. C.; Zadoyan, R.; Kohler, B.; Messina, M. *J. Chem. Phys.* **1997**, *106*, 8486.
(177) Zadoyan, R.; Sterling, M.; Ovchinnikov, M.; Apkarian, V. A. *J. Chem. Phys.* **1997**, *107*, 8446.
(178) Li, Z.; Fang, J. Y.; Martens, C. C. *J. Chem. Phys.* **1996**, *100*, 7873.
(179) Conley, A. J.; Fang, J. Y.; Martens, C. C. *J. Phys. Chem. A* **1998**, *102*, 4291.
(180) Batista, V. S.; Coker, D. F. *J. Chem. Phys.* **1997**, *106*, 6923.
(181) Liu, L.; Guo, H. *J. Chem. Phys.* **1995**, *103*, 7851.
(182) Ovchinnikov, M.; Apkarian, V. A. *J. Chem. Phys.* **1997**, *106*, 5755.
(183) Segall, J.; Wen, Y.; Singer, R.; Wittig, C.; Garcia-Vela, A.; Gerber, R. B. *Chem. Phys. Lett.* **1993**, *207*, 504.
(184) Schroeder, T.; Schinke, R.; Mandziuk, M.; Bacic, Z. *J. Chem. Phys.* **1994**, *100*, 7239.
(185) Schmidt, B.; Jungwirth, P.; Gerber, R. B. In *Femtochemistry*; Chergui, M., Ed.; World Scientific: Singapore, 1996; p 637.
(186) Cooper, A. R.; Hutson, J. M. *J. Chem. Phys.* **1993**, *98*, 5337.
(187) Jungwirth, P. *Chem. Phys. Lett.* **1998**, *289*, 324.
(188) Rabo, J. A.; Angell, C. L.; Kasai, P. H.; Shomaker, V. *Discuss. Faraday Soc.* **1966**, *19*, 328.
(189) Barrer, R. M.; Cole, J. F. *J. Phys. Chem. Solids* **1968**, *29*, 1755.
(190) Westphal, U.; Geismar, G. *Z. Anorg. Allg. Chem.* **1984**, *508*, 165.
(191) Smeulders, J. B. A. F.; Hefni, M. A.; Klaassen, A. A. K.; Boer, E. D.; Westphal, U.; Geismar, G. *Zeolites* **1987**, *7*, 347.
(192) Blake, N. P.; Metiu, H. *J. Chem. Phys.* **1995**, *103*, 4455.
(193) Heller, E. J. *J. Chem. Phys.* **1981**, *75*, 2923.
(194) Blake, N. P.; Metiu, H. *J. Chem. Phys.* **1994**, *101*, 223.
(195) Van Wieringen, A.; Warmoltz, N. *Physica* **1956**, *23*, 849.
(196) Buda, F.; Chiarotti, G. L.; Car, R.; Parrinello, M. *Phys. Rev. Lett.* **1989**, *63*, 294.
(197) Panzarini, G.; Colombo, L. *Phys. Rev. Lett.* **1994**, *73*, 1636.
(198) Langpape, C.; Fabian, S.; Klatt, C.; Kalbitzer, S. *Appl. Phys. A: Solids Surf.* **1997**, *64*, 207.
(199) Forsythe, K. M.; Makri, N. *J. Chem. Phys.* **1998**, *108*, 6819.
(200) Miller, W. H. *J. Chem. Phys.* **1974**, *61*, 1823.
(201) Miller, W. H.; Schwartz, S. D.; Tromp, J. W. *J. Chem. Phys.* **1983**, *79*, 4889.
(202) Schwartz, S. D. *J. Chem. Phys.* **1997**, *107*, 2424.
(203) Stavola, M.; Cheng, Y. M. *Solid State Commun.* **1995**, *93*, 431.
(204) Ben-Nun, M.; Martinez, T. J.; Molnar, F.; Lu, H. *University of Illinois Theoretical Biophysics Technical Report UIUC-TB-98-06*, 1998.
(205) Ben-Nun, M.; Molnar, F.; Lu, H.; Phillips, J. C.; Martinez, T. J.; Schulten, K. *Faraday Discuss.* **1998**, *110*, 447.
(206) Ben-Nun, M.; Martinez, T. J. *J. Phys. Chem. A* **1998**, *102*, 9607.
(207) Pebay-Peroula, E.; Rummel, G.; Rosenbusch, J.; Landau, E. *Science* **1997**, *277*, 1676.
(208) Kimura, Y.; Vassylyev, D.; Miyazawa, A.; Kidera, A.; Matsushima, M.; Mitsuoka, K.; Murata, K.; Hirai, T.; Fujiyoshi, Y. *Nature* **1997**, *389*, 206.
(209) Humphrey, W.; Logunov, I.; Schulten, K.; Sheves, M. *Biochemistry* **1994**, *33*, 3668.
(210) Logunov, I.; El-Sayed, M.; Lanyi. J. *Biophys. J.* **1996**, *70*, 2875.

CR9800210